AD-A062 464 WAYNE STATE UNIV DETROIT MICH BIOMECHANICS RESEARCH --ETC F/G 6/19
BIOENGINEERING MEASUREMENT.(U)
MAR 77 A I KING

UNCLASSIFIED

N00014-75-C-0372

NL

| OF |
AD
A062464

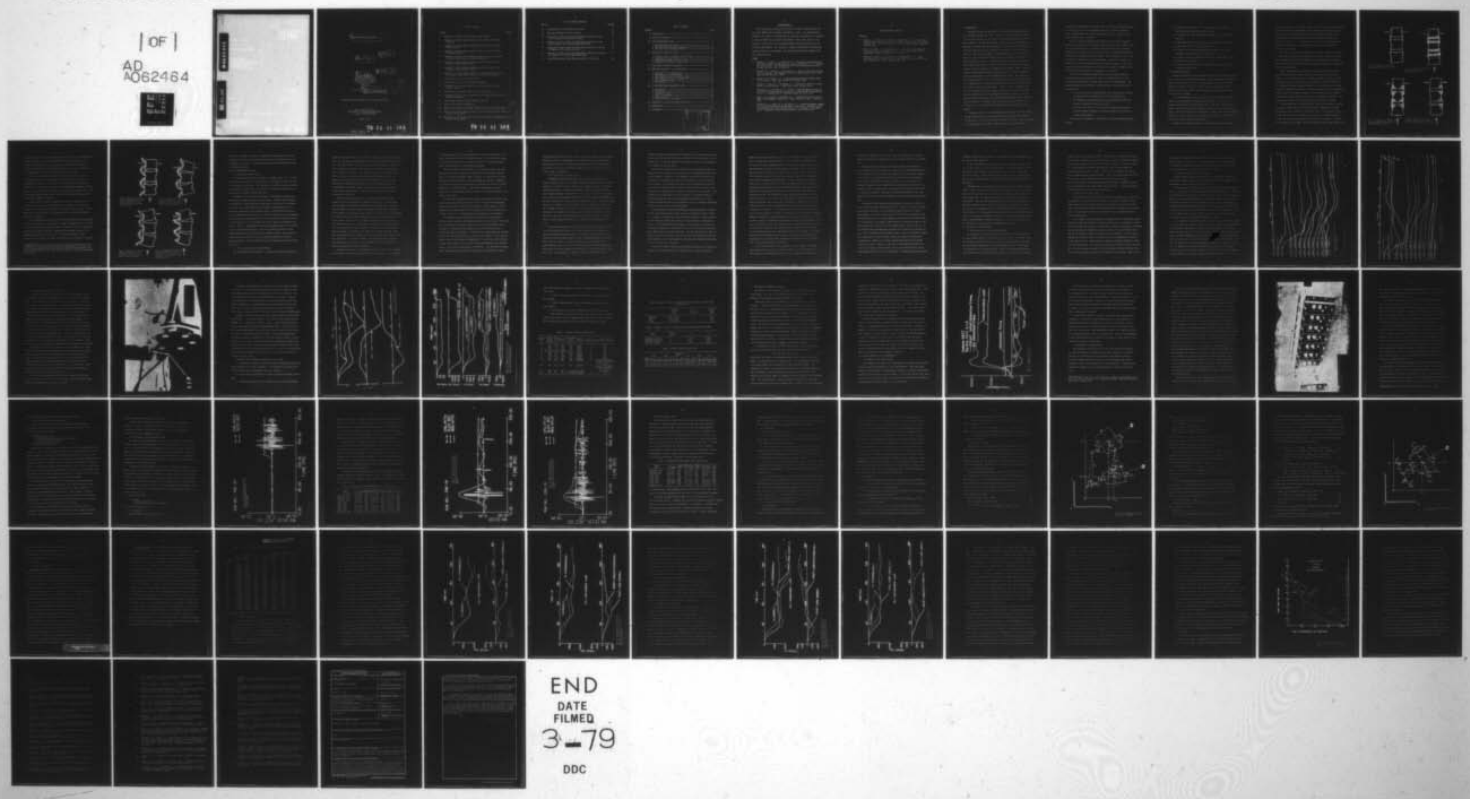

END
DATE
FILMED
3-79
DDC

(6) BIOENGINEERING MEASUREMENT.

by

(10) Albert I. King

(12) 73 p.

(11) 1 Mar 77

(9) Final Report of
Research Sponsored by
DEPARTMENT OF THE NAVY
OFFICE OF NAVAL RESEARCH
Biophysics Program
Code 444

(15) Contract No. N00014-75-C-0372,
N00014-69-A-0223-0001

Approved for public release, distribution unlimited

Wayne State University
Department of Mechanical Engineering
Detroit, Michigan 48202

March, 1977

LIST OF FIGURES

LIST OF FIGURES CONTINUED

TABLE OF CONTENTS

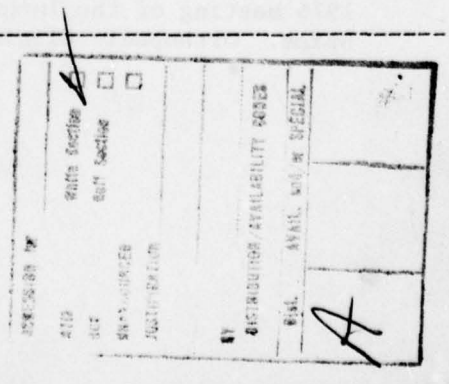

ACKNOWLEDGMENTS

This research was sponsored by the Office of Naval Research under Contract Nos. N00014-69-A-0235-0001 and N00014-75-C-0372. The administrative support of Dr. Arthur B. Callahan and the technical assistance of Dr. Channing L. Ewing of NAMRL are gratefully acknowledged. Much of the work for this study was carried out by Dr. Priyaranjan Prasad under the direction of the principal investigator. Dr. Stephen A. Tennyson contributed to the muscular response portion of the program. The following publications resulted from this research effort:

PAPERS

1. Ewing, C. L., King, A. I. and Prasad, P.: Structural considerations of the human vertebral column under $+G_z$ impact acceleration. J. of Aircraft 9(1):84-90, 1972. Also presented at the AIAA Ninth Aerospace Sciences Meeting, New York, Jan. 25-27, 1971.

2. Begeman, P. C., King, A. I. and Prasad, P.: Spinal loads resulting from $-G_x$ acceleration. Proceedings of the 17th Stapp Car Crash Conf., Oklahoma, pp. 342-360, Nov., 1973.

3. Prasad, P. and King, A. I.: An experimentally validated dynamic model of the spine, J. Appl. Mech. 41(3), pp. 436-550, 1974.

4. Prasad, P., King, A. I. and Ewing, C. L.: The role of articular facets during $+G_z$ acceleration, J. Appl. Mech. 41(2):321-326, 1974.

5. Tennyson, S. A. and King, A. I.: Effect of intra-abdominal pressure on the spinal column during $+G_z$ acceleration. Advances in Bioengineering, Ed. by J. A. Brighton and S. Goldstein, ASME, pp. 95-97, 1974.

6. King, A. I., Prasad, P. and Ewing, C. L.: Mechanism of spinal injury due to caudocephalad acceleration. Orthop. Clinics N. Amer., 6(1):19-31, 1975.

7. Tennyson, S. A., Mital, N. K. and King, A. I.: Electromyographic signals of the spinal musculature during impact acceleration. Presented at the 1976 meeting of the International Society for the Study of the Lumbar Spine. Orthopedic Clinics of North America, 8(1):97-119, 1977.

ACKNOWLEDGMENTS CONTINUED

ABSTRACTS

1. Ewing, C. L., King, A. I., Prasad, P. and Vulcan, A. P.: A method for increasing the threshold level for vertebral fracture due to $+G_z$ impact accelerations. Proc. of the 9th Int. Conf. on Med. and Biol. Engineering, Aug. 1971.

2. Prasad, P., King, A. I. and Ewing, C. L.: The role of the articular facets during $+G_z$ acceleration. Proc. of the 25th Annual Conf. on Engineering in Med. and Biol., Oct. 1-5, 1972.

3. Prasad, P., King, A. I., Denton, R. A. and Begeman, P. C.: Intervertebral force transducer. Proc. of the 10th Int. Conf. on Med. and Biol. Engineering, p. 137, Dresden, GDR, 1973.

I. INTRODUCTION

Vertebral injuries are sustained by crewmen during emergency egress from disabled high-speed aircraft. These aircraft have been in existence for over three decades and there have been numerous ejections by pilots of many countries. In these thirty years, there has also been remarkable advances in aircraft and space technology. However, progress in the area of injury reduction in pilot ejection has been slow. One of the major factors for the lack of progress is the assumption that the spine is required to carry the inertial load of the torso, proportional to the acceleration level of the seat, and that there is very little anyone can do to reduce this load for a given acceleration. This concept is quite evident in the early models for simulating the ejection event. Latham (1) assumed a lumped parameter base excitation model in which the torso or mass was placed above a spring representing the spine. The assembly was accelerated upward by a force or acceleration pulse applied to the bottom of the spring and the resulting peak force in the spine was greater than the product of mass and acceleration. It was, in fact, dependent upon the rate of onset of the input pulse. Conceptually, this model provided an over-simplification of the problem and stifled any ideas of load reduction borne by the spine. The continuum model proposed by Hess and Lombard (2) was also too simple, since it simulated the acceleration of a straight rod or column which had a uniform weight distribution along its length.

Subsequent models by many investigators perpetuated the axial loading concept and reduction of injury was not achieved through these efforts. In 1968, King et al (3) proposed and verified the hypothesis that the spinal column carried an eccentric load, and that it was subjected to

a simultaneous compressive and bending load. The basis for this hypothesis was strain gage data from instrumented vertebrae of embalmed cadavers which were subjected to $+G_z$ impact accelerations, using a vertical accelerator at Wayne State University.

Dr. C. L. Ewing of NAMRL had been interested in the pilot ejection problem and had observed that anterior wedge fractures were a common injury mode in pilots who eject. He proposed a hypothesis that the posterior structure of the spine acted as a motion limiter, preventing spinal hyperextension, but facilitating spinal flexion. Ewing proposed to verify this hypothesis by putting the spine into moderate extension to position the vertebrae in a less favorable position for anterior wedging. It was reasoned that posterior compression of the vertebral column is limited by the articular facets while anterior compression is unlimited.

In view of the observed bending effects and the Ewing hypothesis, a research project was conceived to verify the hypothesis and to study the precise mechanisms of vertebral injury due to $+G_z$ acceleration. The proposed sponsor was the Office of Naval Research. The specific aims of the study were:

1. To verify that spinal hyperextension will reduce strain along the anterior aspect of vertebrae in the thoraco-lumbar spine.
2. To determine the extent and manner of hyperextension which will produce the maximal reduction in strain.
3. To verify that there is a statistically significant increase in fracture g-level sustained by cadaveric subjects as a result of spinal hyperextension.

Upon sucessful attainment of these aims, the following objectives were pursued:

4. To quantify the existence of a facet load which constituted a second load path along the vertebral column.
5. To identify the role of abdominal pressure as a possible third load path.
6. To determine the effect of the spinal musculature on vertebral column response due to $+G_z$ acceleration.
7. To develop a two-dimensional mathematical model of the spine simulating its response to $+G_z$ acceleration.
8. To conduct cadaveric experiments which will provide data for the validation of this model.
9. To propose this model for the assessment of injury probability in ejection seat design.

II. THE EWING HYPOTHESIS

Several hypotheses have been advanced to explain these vertebral fractures. Most of the proposed explanations concern simply peak acceleration values, and peak rates of onset of acceleration, and view the vertebral column as a single structure or series of single structures having a physical failure point, which, when exceeded, causes structural failure of one or more vertebrae.

It is hypothesized by others, however, that such structural failure limits can be increased by altering body positioning. In this view, opening the angle that the longitudinal axis of the torso forms with the vertical axis of the unrestrained pelvis, by means of increasing the seat angle, will prevent fracture, by arranging the impact vector of the ejection thruster so that it does not occur normal to the superior or inferior surface of the thoraco-lumbar vertebral bodies.

Ewing et al (4) proposed that one of the major causes of ejection

vertebral fracture is the dynamic reaction of the vertebral column under $+G_z$ (eyeballs down) impact acceleration in the presence of improper restraint; that is, there are certain movements of the individual vertebral bodies under $+G_z$ impact acceleration that cause the characteristic ejection vertebral fracture. If this theory is correct and if these motions are prevented, the fractures would therefore be expected to occur only at markedly higher levels.

This may be explained by considering the vertebral column as a series of spring-mass systems, with the intervertebral disks serving as springs, the vertebral bodies (and body segments that they support) as individual masses, and the anterior and posterior interspinous ligaments as spring limiters (on tension only).

Figure 1 demonstrates an idealized vertebral segment consisting of three vertebrae acting as masses and two intervertebral disks acting as springs. If this segment acted as a simple spring-mass system, an impact acceleration in the vector normal to the superior or inferior surface of the vertebral bodies and passing through the center of mass should result in plateau compression fracture(s), as noted in Figure 2, if the compression failure limit of the superior surface of the vertebral body is exceeded. (Acceleration vector direction is shown in the figures by an arrow). Such fractures are rarely seen in ejection vertebral fractures, however.

If an acceleration is applied with the vector either before or behind the center of mass, anterior or posterior wedge compression fractures, respectively, should result if the failure limit of the superior surface of the vertebral body is exceeded due to anterior or posterior bending of the multiple spring-mass system, as illustrated in Figure 3. However, recent examination of eighty ejection vertebral fracture cases by Ewing (5),

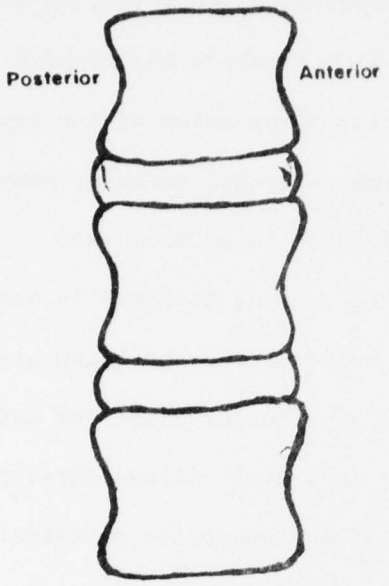

Fig. 1 Diagram of a typical thoraco-lumbar spinal segment.

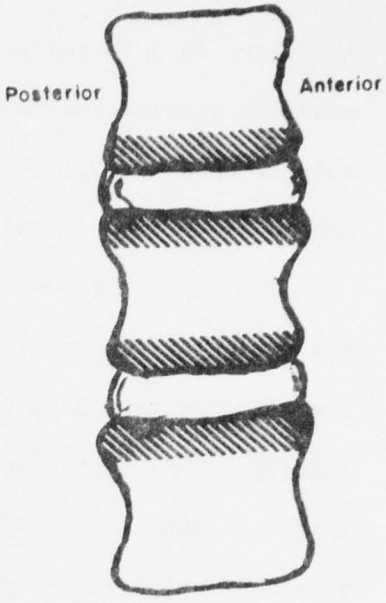

Fig. 2 Diagram of a spinal segment showing areas affected by plateau fractures

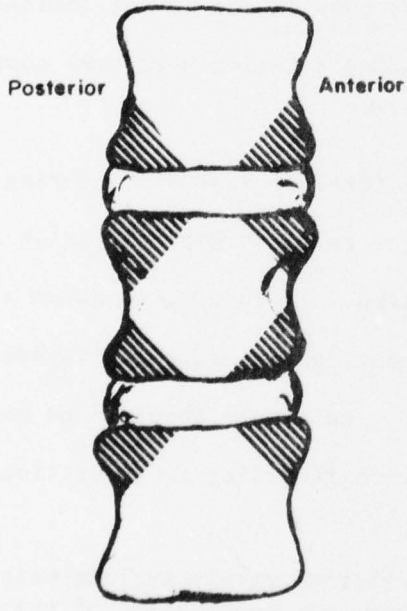

Fig. 3 Diagram of a spinal segment showing areas affected by compression fractures.

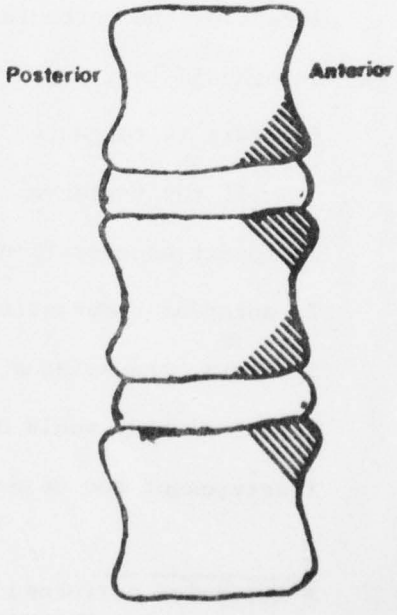

Fig. 4 Diagram of a spinal segment showing areas affected by ejection vertebral fractures.

showed that almost all were anterior compression fractures, as demonstrated in Figure 4; only one posterior compression fracture was found.* One possible explanation is that the posterior compression of the system is subject to some spring-limiting mechanism, whereas, anterior compression is not. Examination of the anatomy reveals this to be the case.

The posterior compression limiter (or spring limiter) is seen to be the articular facets of the vertebrae, held together by ligaments, as demonstrated in Figure 5, that serve as a posterior hinge for adjacent vertebrae. As can be seen in Figure 6, this hinge allows anterior vertebral lips to touch but prevents any contact of the posterior vertebral lips. Thus an additional spring-limiter system other than the anterior and posterior interspinous ligaments is acting.

An hypothesis is therefore presented; posterior compression of the vertebral column in the thoraco-lumbar area is limited by the articular facets of the vertebrae while anterior compression is not limited. If this hypothesis is true, a means of preventing anterior vertebral compression fracture is suggested.

If the vertebral column could be forcibly restrained during application of impact acceleration in a position of relative hyperextension as in Figure 7, anterior compression would be limited. Therefore, to cause a compression fracture, the spinous processes connecting the articular facets to the vertebral body would have to be torn. The forces required to cause fractures of the spinous processes with restraint in a position of hyperex-

---

* Autopsies performed on ejection fatalities rarely include vertebral body examinations. The conclusion was based upon examination of the x-ray report in each instance of those confirmed by x-ray as having suffered a vertebral fracture and survived. Those fatally injured at time of ejection were not included.

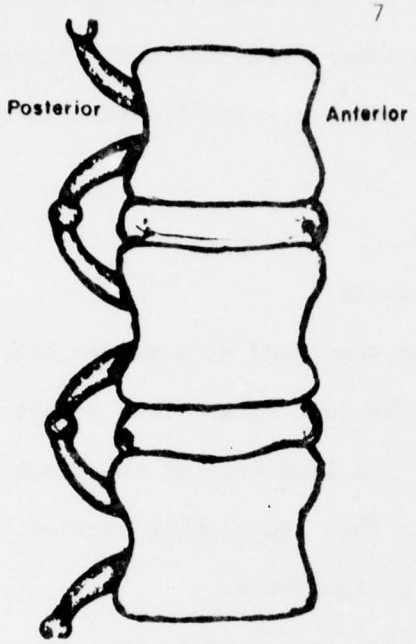

Fig. 5 Diagram of an erect spinal segment showing the relative position of the articular facets and spinous processes.

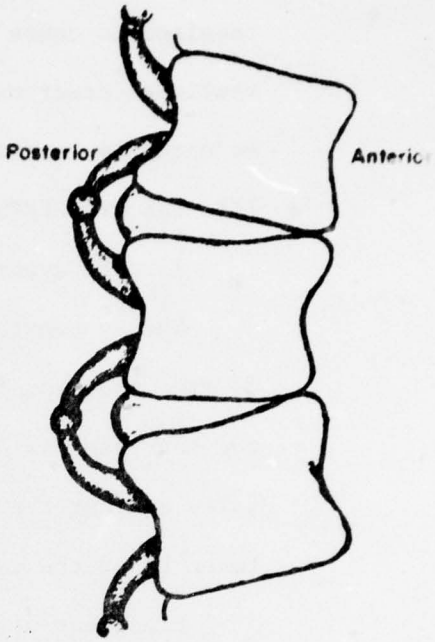

Fig. 6 Diagram of a spinal segment showing relative positions of the vertebral bodies during flexion.

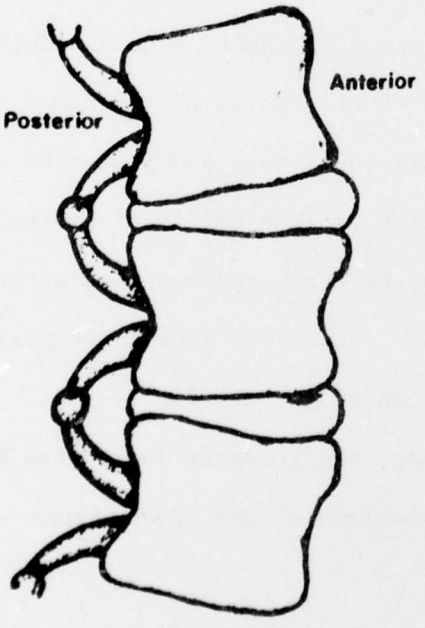

Fig. 7 Diagram of a spinal segment showing relative positions of the vertebral bodies during extension.

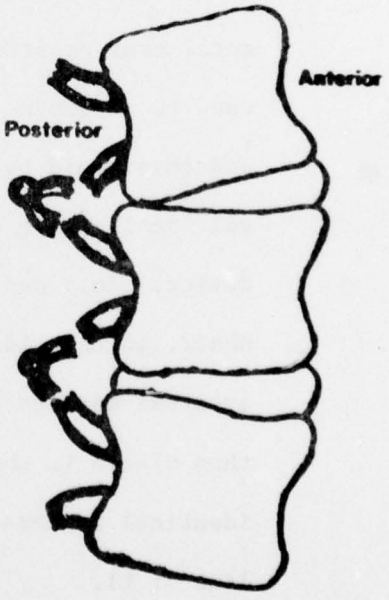

Fig. 8 Diagram of a spinal segment showing the mechanism required to permit posterior compression fractures of the vertebral bodies

tension as in Figure 8, would be increased quite considerably over those required to cause anterior vertebral fracture while restrained in the conventional erect manner. Thus the vertebral fracture threshold limit would be markedly increased.

III. THE HYPEREXTENSION TESTS

1. The Hyperextension Device

The hyperextension device consisted of a wooden block, 15 cm x 10 cm x 57 cm, that was fastened to the seat back. The height of the block from the seat pan was adjustable. The long axis of the block was placed horizontally against the seat back so that the block's smallest dimension was between L1 of the cadaver and the seat back.

Placement of the blocks was determined by experiments carried out to determine the optimal location, size and shape. Based on those findings, the centerline of eack block was placed opposite the body of L1 in almost all cases. Due to the difficulties inherent in performing x-rays on a metal seat positioned over an elevator shaft, a wooden mock-up seat was used to determine the location of L1. While L1 was known to be instrumented and this could be detected easily on x-ray, the posterior exterior anatomical localization of L1 was necessary in order to place the hyperextension device. This was accomplished by using radio-opaque markers on the wooden chair, in the midsagittal plane. The x-ray showed the position of the external markers and the position of L1 relative to them. The cadaver was then placed in the ejection seat, the geometry duplicated by means of identical markers, and the centerline of the block placed next to the centerline of L1.

2. The Vertical Accelerator Experiments

All experiments were performed on a vertical accelerator housed in an

eight-story elevator shaft of the School of Medicine at Wayne State University. The sled has an aircraft ejection seat mounted directly above the piston. The angle between seat pan and seat back is 90 degrees. Accelerator line of thrust is parallel to the seat back. The cadaver was positioned in the seat prior to firing. The acceleration pulse was induced with the sled at rest at the bottom of the shaft; stroke length is 2.44 m. At completion of the input acceleration pulse, braking was initiated and deceleration completed within about 12 m. The acceleration pulse was approximately trapezoidal in shape, the rate of onset and the magnitude of the plateau being variable. Details of the accelerator have been described by Patrick (6).

Foil-type strain gages, 0.125 in. in length, were bonded to the cleaned surfaces using Eastman 910 adhesive and catalyst. Strain gages were installed on the anterior surface of the vertebral body in the midsagittal plane, and lateral gages were mounted in bilaterally symmetrical pairs coplanar in the coronal plane of T12, L2, and L4 on two of the cadavers. One cadaver also had an anterior gage on L1 and two posterior gages on L2. On the other 8 cadavers, the only gages installed were anterior ones on each vertebra from T11-L4. On the last 2 cadavers, only an anterior gage on L4 was installed, in order to preserve the integrity of the anterior spinous ligament, as a control. All gages were applied with their sensitive axes parallel to the vertical axis of the vertebral body, and all leads were presoldered to the gage terminals. An attempt was made to install these gages near the neutral axis of the vertebra so that their output indicated predominantly axial compression.

The gages were tested, and a minimum of 500 MΩ of resistance to ground was obtained to ensure long-lasting and noise free outputs. After testing

for proper operation, the installed gages were coated with Gagekote #3 to insure insulation from body or embalming fluids. The leads from the gages were attached by sutures to an adjacent body part to prevent accidental removal during exposure to experimental conditions.

After the cadaver was positioned in the accelerator chair, the leads from the lateral strain gages were connected to form diagonally opposite arms of a four-arm Wheatstone bridge; the other two arms were 121-Ω high-stability precision resistors. This configuration resulted in summing of the output of the left and right gages to eliminate the effects of lateral bending of the vertebral column. The anterior gage formed a two-arm bridge with a 121-Ω resistor, with the other two arms being provided by the bridge balance unit.

The following gage indentification symbols were used: the prefix A denoted a gage on the anterior surface of T12. The prefix D denoted gages mounted on the lateral surface of the vertebra. Strain values of DL2 represented the average output of the two gages on the lateral surface of L2 on either side of AL2. Posterior gages were denoted by the prefix DD.

The restraint system consisted of an automotive lap belt under a regular aircraft lap belt and shoulder harness, with leg straps. The wrists were tied together and loosely anchored to the seat base without tension by means of a single rope run through an eye bolt in the seat base to prevent flailing of extremities. A rope was also looped around the aircraft lap belt and through the eye bolt to serve as an inverted V. This step was taken so that no load would be transmitted to the arm rest, and to prevent vertical displacement of the lap belt during pretensioning of the shoulder harness, and during the experimental acceleration. The lap belt was always snugly tightened, and the shoulder harness was then preloaded to a 89 N

tension before each run except for those runs in the flexed mode (vide infra). Although the head was unrestrained, its initial position was kept approximately vertical by means of masking tape that broke once the head started rotating but did not have sufficient breaking strength to serve as a motion limiter under acceleration.

3. Fracture Levels and Spinal Modes

Instrumented cadavers restrained in the seat were subjected to $+G_z$ impact accelerations in 3 g-4 g (peak) increments, keeping the rate of onset constant at roughly the rate of onset of the standard ejection seat (approx. 300 g/sec-500 g/sec). The input acceleration pulse was trapezoidal, with peak plateau amplitudes varying from 5.5 g to 24.5 g. Duration of the input pulse varied from approximately 140 m/sec to 300 m/sec and was dependent upon the peak acceleration, since total stroke length was 2.44 m. After each impact exposure, the cadaver was x-rayed again, and if no fracture was noted, the next incremental exposure was given. In some cases, the x-rays were developed after the completion of several runs. If fracture occurred in one of these runs, the data from all postfracture runs were discarded. The end point for each cadaver was fracture of a vertebral body demonstrable by x-ray.

At each peak acceleration level, the cadaver was tested in one or more of the following spinal modes: 1) the entire thoraco-lumbar segment was forced into moderate hyper-extension and maintained in this position by the restraint system and hyperextension device--the extended mode; 2) the vertebral column was allowed to assume the normal erect configuration of a seated cadaver, with a lap belt and shoulder harness restraint system--the erect mode; and 3) the cadaver was restrained in a seated position by a lap belt only. In the absence of a shoulder harness, hyperflexion of the

vertebral segment was permitted--the flexed mode. On some cadavers anterior strain gages were used on all vertebral bodies from T11 through L4, but on controls only L4 was instrumented to determine the effect of instrumenting the vertebrae on fracture level.

The effect of evisceration on fracture level and measured strain was tested on the two cadavers on which only L4 was instrumented and which were not eviscerated. Retention of the abdominal viscera can only affect the fracture level adversely since some of this weight must be borne by each spinal segment. To determine the effect of the experimental acceleration as a cause of fracture, precise fracture timing relative to onset of sled acceleration by examination of vertebral body strain curves was used. From postrun x-ray studies alone it was not possible to determine whether a detected fracture was due to the experimental acceleration, or to the braking deceleration which may be considered as only a necessary experimental evil, and not a factor in the experiment.

The experimental design and resulting acceleration levels at fracture as well as the spinal mode in which fracture occurred are listed in Table 1. A summary of average peak sled acceleration required to cause fracture for all modes and average age at death of those cadavers is contained in Table 2. The extended mode shows roughly a 50% increase in the peak sled acceleration required to cause fracture over the level for the erect mode, and a 100% increase over the flexed mode. Yet the seat angle, the line of thrust relative to the pelvis, and the cadaveric back structure itself were all unchanged, and the instrumentation and cadaveric preparation were identical in the majority of the runs.

Reference to Table 1 reveals that the peak acceleration at fracture for cadaver 11 in the extended mode is unknown since no fracture occurred,

despite peak sled acceleration of 24.5 g. Yet no cadaver run in either the erect or flexed mode escaped fracture. More importantly, examination of the time of fracture (determined from the strain gages) shows that all erect and flexed mode fractures occurred within the duration of the sled experimental acceleration pulse, while none of the extension mode fractures definitely occurred during this period, and only one (cadaver 12) could have occurred during experimental acceleration. Instead, examination of Table 1 shows that for cadavers 9 and 10, run in the extended mode, the vertebral fractures occurred after the end of sled acceleration and thus well into the period of the braking deceleration pulse; and therefore, these present a different problem. The deceleration pulse, which was necessarily used for these experiments due to location of the accelerator device, does not occur during operational ejection seat use. Therefore, a fracture due to the deceleration event is only an experimental artifact with regard to the input acceleration of interest. The deceleration fractures that occurred to cadavers 9 and 10 apparently were due to the disruption of the anterior vertebral ligament incidental to instrumentation of the anterior vertebral bodies T11-L4, which altered the vertebral column dynamic response on deceleration. The time of occurrence of the other fracture in the extended mode (cadaver 12) is not known, and, therefore, has been arbitrarily assigned to the group due to the acceleration pulse for conservative analysis of the data. The difference between the average fracture levels in the erect and flexed modes as compared with the extended mode, therefore, could possibly be more significant if the reverse assignment were made.

A t test was performed for the fracture g levels between the various spinal modes and the results are given in Table 3. The differences in g level between the extended mode and the other two modes were found to be

statistically significant ($P = 0.05$). The null hypothesis was rejected despite conservative estimates made for the fracture level in the extended mode.

When the fracture g levels in the various modes were analyzed, it was not possible to use paired sets of data; so, the appropriate values of t were obtained from the equation for unpaired data with unequal samples. In particular, for extended mode the four fracture levels were obtained under slightly different conditions, in that in two of the cases the anterior ligament was left intact while it was disrupted in the other two. Similarly, when the cadaver was not eviscerated, the fracture level would be expected to decrease. Therefore, the actual difference and the probability that it did not occur by chance can only be higher than those given here.

Comparison of the fracture levels obtained in this series (Table 2) must be made with those reported by Ruff (7). Table VI-8 from his chapter shows maximum tolerance of the individual vertebrae for T12-L1 tested approximately in the erect mode to be 24.5 g and 23.0 g, respectively, and minimum tolerance for the same vertebrae as 18.6 g and 18.2 g respectively. Yet the findings in the present study indicate an average tolerance in the erect mode of 10.4 g $\pm$ 3.79 g in the extended mode of 17.5 g $\pm$ 5.55 g. It is believed that this seeming inconsistency can be resolved on the basis of age. Ruff's specimens were obtained at least in part from accident victims. It is presumed that those accident victims were youthful, whereas the average age of cadavers in the erect and extended modes of the present study was 61 years. Figure 7 of the study by McElhaney and Roberts (8), shows that strength of the vertebral body in the sixth decade of life is approximately half that in the second decade. Empirical data from aircraft

accidents indicate that the majority of individuals suffering vertebral fracture are in their twenties.

If this relationship holds true, therefore, the average fracture level for the erect mode at age 20, which is the one of interest extrapolated from the present study, would be roughly 20 g-25 g and for the extended mode would be 35 g-44 g. Since cadaveric bone is not as strong as living human bone or fresh cadaveric bone, the comparison becomes potentially even more meaningful.

Roentgenograms of the fractures occurring to various cadaveric subjects showed anterior compression fractures for two cadavers tested in the flexed mode; for two cadavers in the erect mode. The fractures that occurred in the extended mode, two cadavers were different from those in the erect or flexed mode. They were somewhat unexpected from previous pathological data and were apparently due to tension on the superior end plate of the vertebral body by the attachment of the intervertebral disk and/or ligament to the end plate. If the hypothesis being tested were true, no fractures would occur in the posterior vertebral structures. This was verified since there was no roentgenographic evidence of damage to the posterior structures of the vertebrae for any experimental acceleration exposure.

IV. THE ROLE OF ARTICULAR FACETS

1. Seat Pan Load for Different Spinal Modes

The hyperextension experiments not only verify the Ewing hypothesis, but also yielded important strain data as shown in Table 4. In many cases, the decrease in anterior strain is a result of hyperextending. The spine is statistically significant at the 95% confidence level. This decrease is attributable to two possible causes. First, the hyperextension device could interact with the torso and carry some of the inertial load and thus

produce a drop in the anterior strain. Alternately, the posterior structures of the spine, principally the articular facets, could be load-bearing elements and provide a second load path for the vertebral column. The first possibility was eliminated by comparing the seat pan loads of hyperextended and erect runs made at the same g level. The traces were identical as long as the run conditions were repeated exactly. Thus, the hyperextension block did not carry part of the inertial load, and that the spinal load was merely redistributed. The Ewing hypothesis could then be extended to state that the articular facets constituted a second load path. The quantification of this facet load is described in this section.

2. Anatomy of the Facet Joint

In a typical vertebra, the articular facets or processes are located near the junction of the pedicles with the lamina. The pair of superior facets spring upward from the pedicles and face in the general posterior direction, while the two inferior facets project downward from the lamina and face anteriorly. The articular surfaces are lined with hyaline cartilege and form a plane synovial joint.

It is obvious from this anatomical arrangement that the overlapping facets perform the important function of limiting rotation and of preventing one vertebra from sliding with respect to its adjacent vertebrae. The question of whether they are capable of transmitting compressive loads in the longitudinal direction of the vertebral column has never really been answered. In most texts of anatomy, the vertebral body is considered to be the weight-bearing structure of the column (9, 10). These references exemplify opinions expressed in 1948 and 1970, respectively. The facets have been said to carry no load at all (11, 12). On the other hand, Strasser (13) and Nachemson (14) have indicated that the facets can support a portion of the load borne by the spine. However, in a

later paper, Nachemson (15) retracted his earlier statement and declared that the facets carry no load. His studies were based on the measurement of intradiscal pressures in isolated spinal segments which were subjected to axial loads while the disk was tilted up to 5 degrees.

3. Qualitative Evidence of Facet Loads

Several techniques were used to deduce the load-bearing capability of the articular facets, since direct measurement of force in a limited space environment is still beyond the state of the art.

Strain gages were an effective means of providing a qualitative indication of facet load. They were mounted on the pedicles and lamina. Methods of installing them on vertebral surfaces were developed to allow the measurement of strain just about anywhere on the external surface of a vertebra. A detailed description of the techniques used to install strain gages on vertebral bodies has been described above. The same methods were employed for installing them on the pedicles, for which an anterior approach is used. To mount them on the posterior surface of a lamina, a posterior approach was taken, but the basic techniques remained unchanged.

As an example of qualitative evidence of facet loads, the strain records of two 8 g runs are compared. Figure 9 shows the anterior (A) and posterior (P) strain gage output with the spine in the erect mode. The posterior gages were installed on the lamina of T10, T11, and L2. Those on T10 and T11 were in tension throughout the pulse while PL2 [illegible]ially in compression and went into tension at about 50 ms after [illegible]set of acceleration. Data from an identical run but with the spine hyperextended are shown in Figure 10. PL2 remained in compression for the entire duration of the pulse, while PT10 and PT11 underwent a change in sign from compression to tension. A marked reduction in anterior strain is also quite evident.

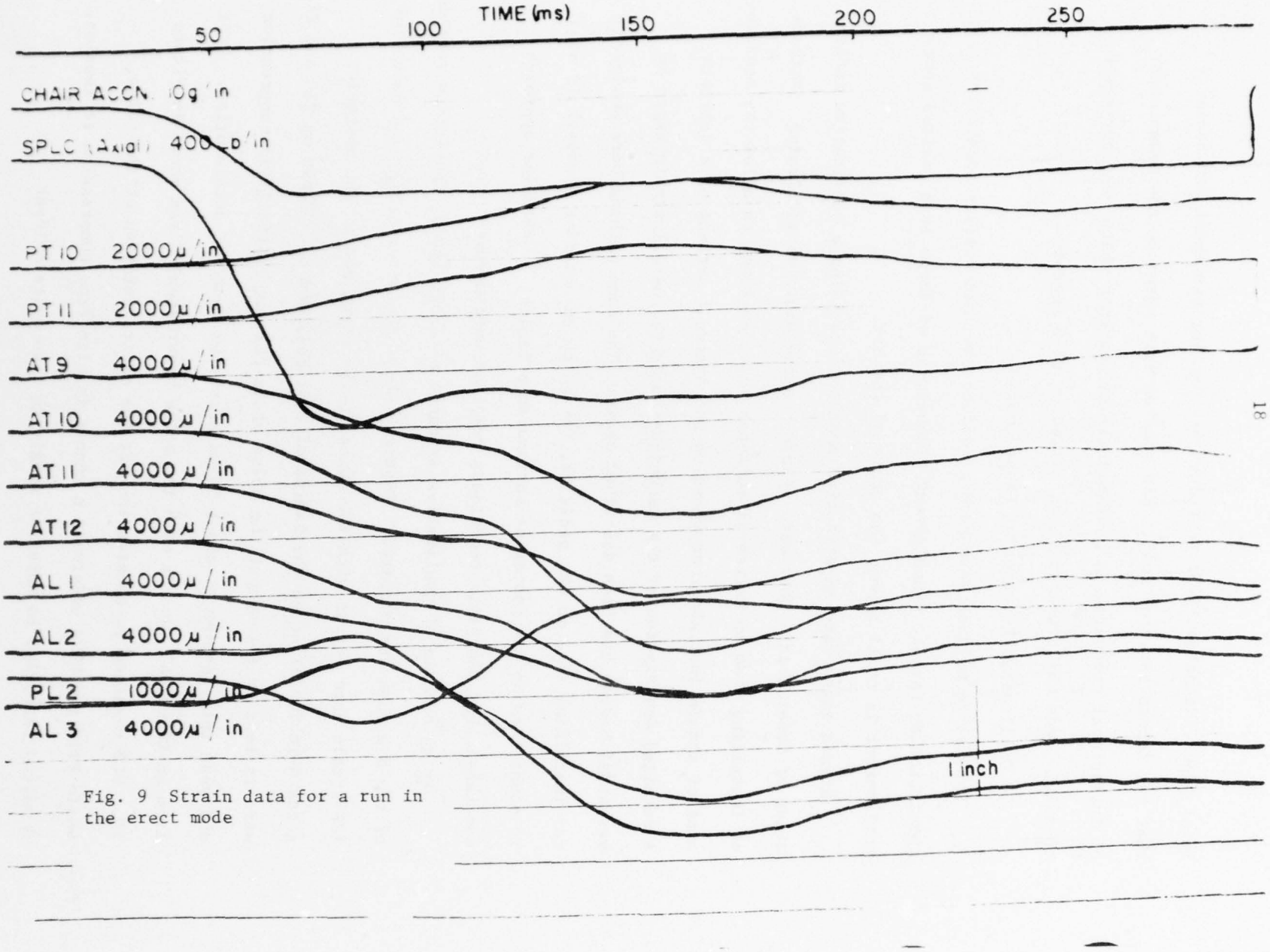

Fig. 9 Strain data for a run in the erect mode

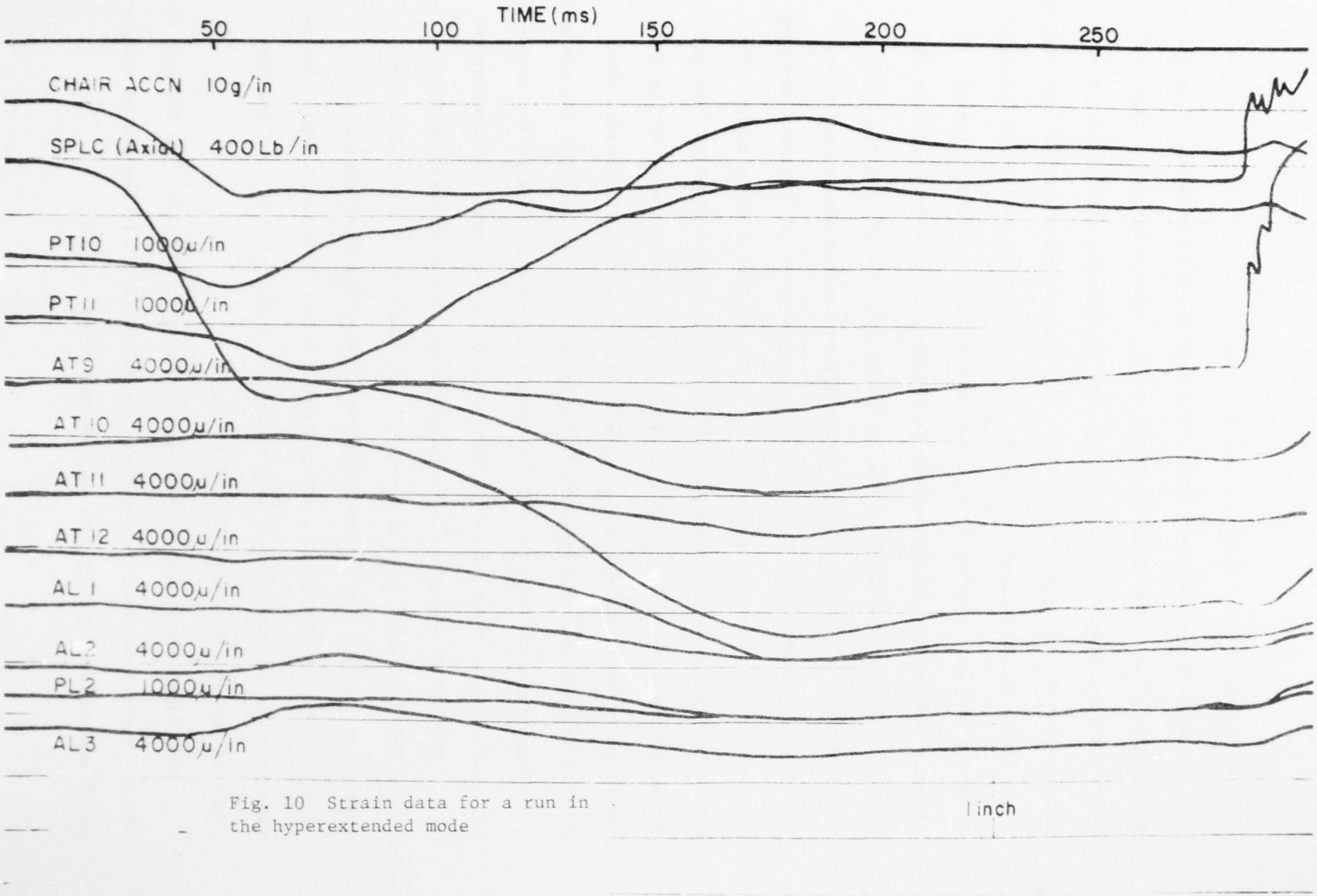

Fig. 10 Strain data for a run in the hyperextended mode

4. Quantitative Evidence of Facet Loads

Quantitative measures of facet load were obtained by means of an intervertebral load cell (IVLC) designed to fit under a disk of a vertebral body. It can measure both axial force and the eccentricity of that force with respect to its geometric center. The first model of an IVLC was almost 1 in. thick and is believed to be the first transducer capable of actually measuring the load carried by a vertebral body in an intact vertebral column. A thinner version is shown in Figure 11. This load cell was designed to fit above a lumbar disk, replacing the inferior segment of a vertebral body. A double-bladed rotary saw was constructed to cut slots of a precise width across the spine to accomodate the IVLC without damaging the neural arch. The lip shown in Figure 11, enables a strap to hold the IVLC in place during the experimental run. A properly installed IVLC will not result in a change in length of the vertebral column, and, if the thinner model is used, the mobility of the column is also not affected. When an IVLC is used, strain gages are installed on both the anterior and posterior.

The purpose of the IVLC was to measure the load carried by the vertebral body and to compare it with that borne by the column, the total spine load. The latter was taken to be proportional to the measured seat pan load. The ratio used was the weight of the torso above the IVLC to the total body weight. Any difference between the spine load and the IVLC output is the load carried by the articular facets, the facet load. Justifications for the validity of this method of deducing facet load are provided in the discussion section of the paper.

IVLC data were obtained from three different cadavers. The initial thicker version was used in the first two cadavers, while the second thinner model was employed during runs made on the third.

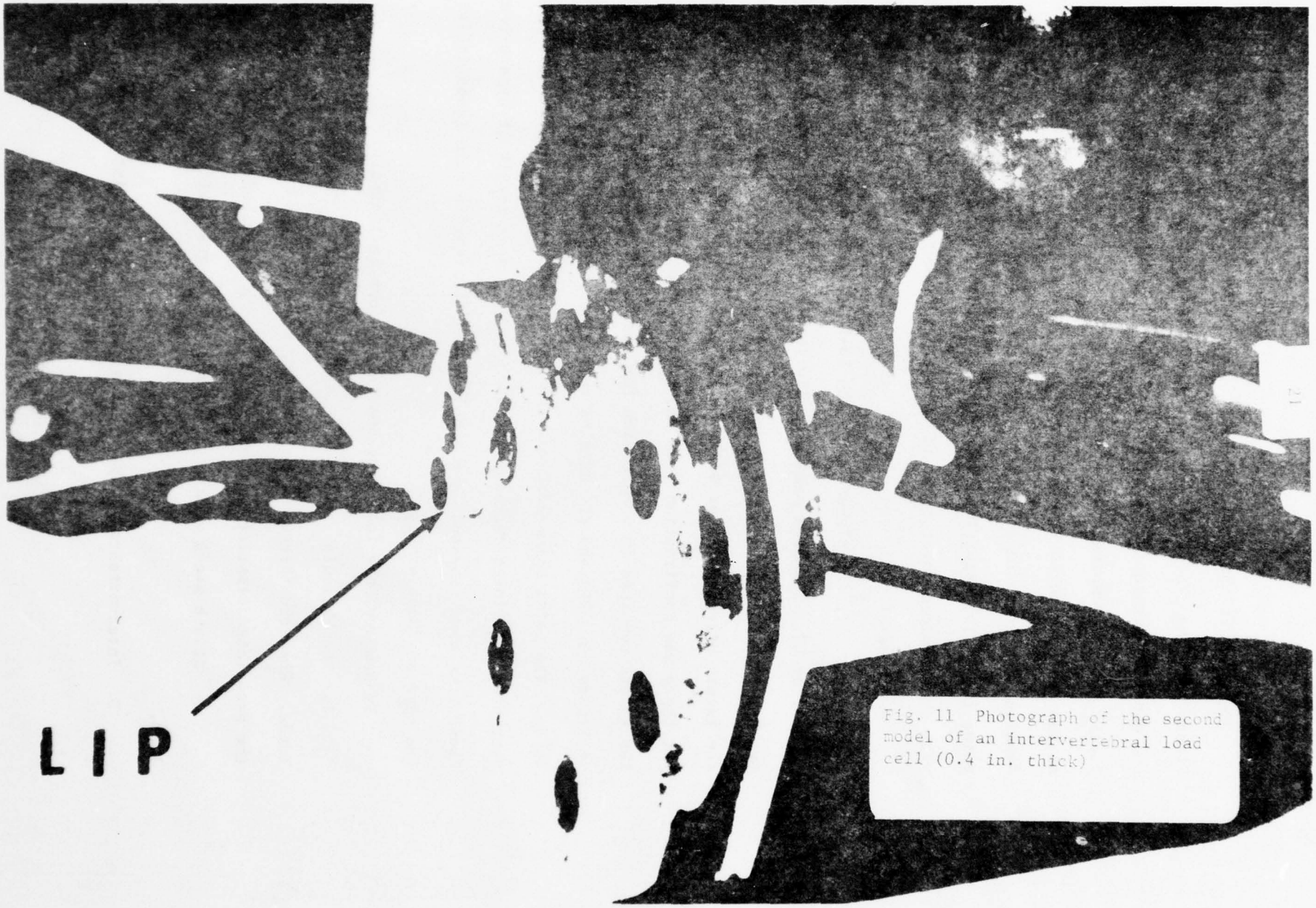

Fig. 11 Photograph of the second model of an intervertebral load cell (0.4 in. thick)

The various spinal loads for a 10 g run in the erect mode are shown in Figure 12. The IVLC replaced the inferior portion of the L3-L4 disk and the superior segment of L4. The neural arch of L4 was left intact. The facets were in compression for the first 125 ms of the pulse. However, as the head and torso rotated forward, the facets unloaded and went into tension, resulting in an intervertebral body force larger than the total spine load. The facet load and PL3 strain also show good correlation, with the zero crossover point of both traces occurring almost simultaneously.

A series of runs were carried out in a cadaver using the thinner model of the IVLC. It was placed about the L3-L4 disk by replacing the inferior segment of L3. The disk was virtually intact. Figure 13 shows data from two 8 g runs made in the erect and hyperextended mode. In the first case the facets unloaded rather early in the acceleration pulse (at about 60 ms) but there was confirmation from PL3 strain. In the hyperextended mode, the facets remained in compression for the entire pulse duration, as shown in Figure 13. PL3 and PL4 strains were also in compression throughout the pulse. The total spine load was the same in these two runs, but the intervertebral body force decreased by about 400 lb as a result of hyperextension. These runs were repeated at 6 and 10 g and the results were essentially the same as those at 8 g.

In summary, the following conclusions can be listed:

1. The articular facets are capable of bearing compressive and tensile loads. When the facets are in tension, it is assumed that the joints and the associated capsular attachments are being stretched.

2. Strain gages were employed to provide qualitative evidence of facet load.

3. Intervertebral body force was measured in an intact spine during

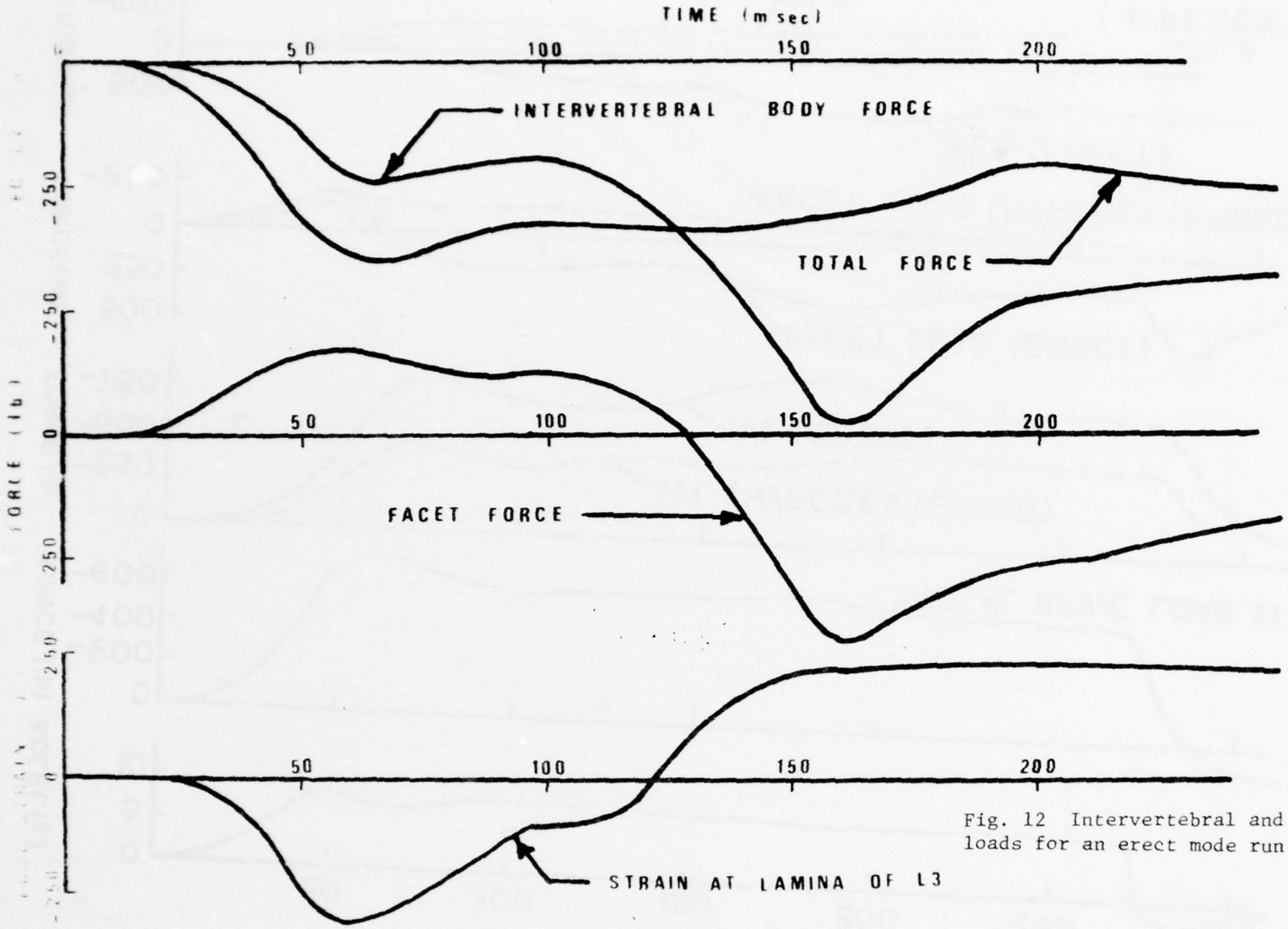

Fig. 12 Intervertebral and facet loads for an erect mode run

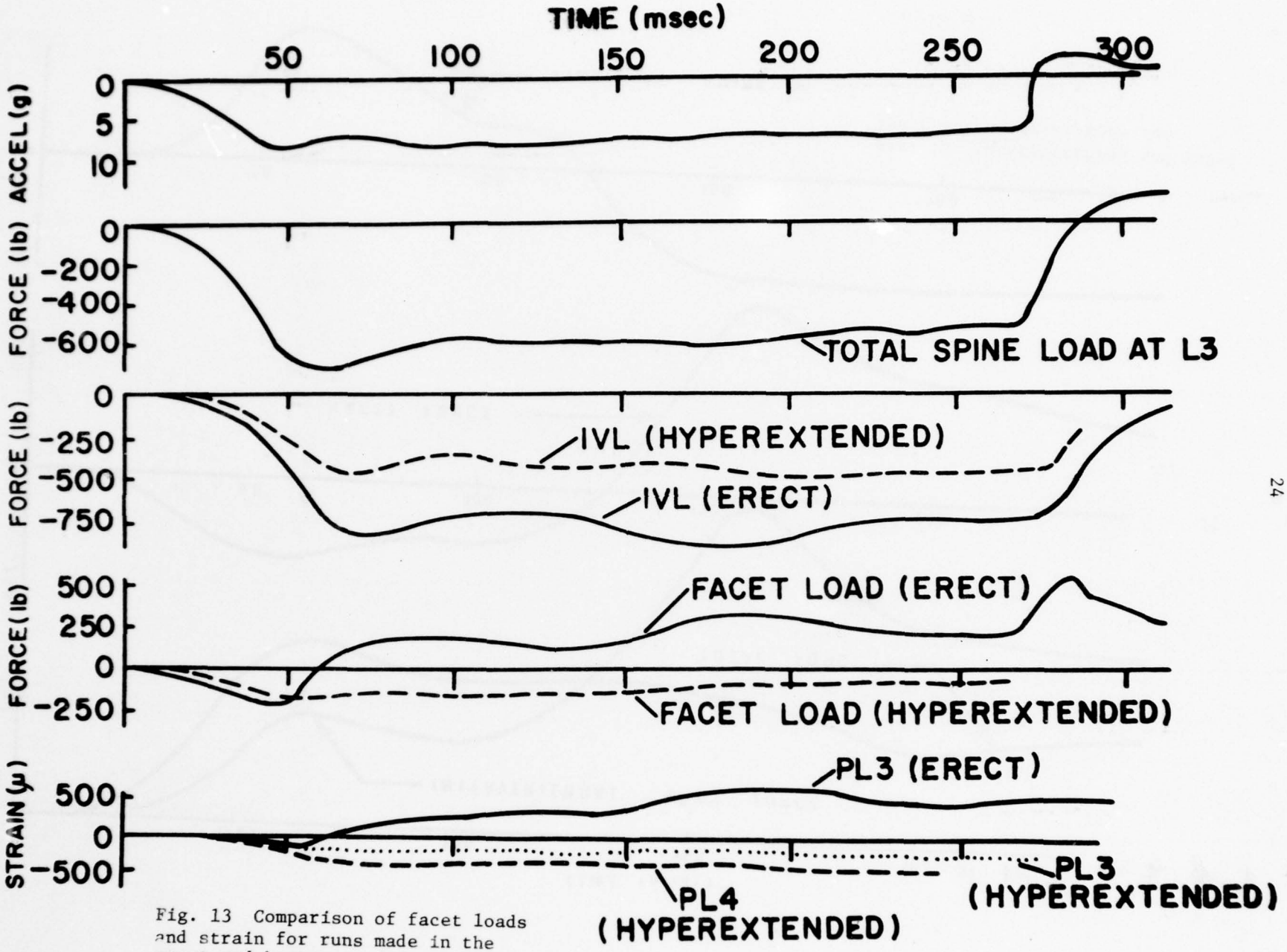

Fig. 13 Comparison of facet loads and strain for runs made in the erect and hyperextended modes

impact acceleration by means of a specially designed intervertebral load cell (IVLC).

4. From the IVLC and seat pan load cell output, a facet load history was computed.

5. A better understanding of the injury mechanism of the spine has been achieved.

6. Hyperextension of the spine transfers more load to the facets.

7. The proportion of the load carried by the facets appear to increase with the decreasing g levels, suggesting that they may also carry a portion of the static body weight when the body assumes normal erect posture.

Table 1 Fracture Levels and Spinal Modes

Cadaver No.	Rate of Onset (g/sec)	Peak Accl. (g)	Duration (m/sec)	Time After Onset (m/sec)	Mode At Fracture	No. of Modes Tested	Fractured Vertebra
1	246	11.0	195	116	erect	2	T12
2	320	7.5	238	138	erect	2	T10
3	375	5.5	300	130	erect	2	T11
4	Data Lost	14.0	Data Lost	110	erect	2	T9
5	418	14.0	208	60-140	erect	2	T11
6	830	7.0	263	120	flexed	3	L2
7	162	11.0	248	85	flexed	3	T11
8	333	9.0	245	195	flexed	3	L2&L4
9	267	14.0	206	390	extended	1	Tension fracture on superior end plate of L1
10	483	20.0	170	290	extended	1	Tension fracture on superior end plate of T12 & L2
11	280	24.5	140	no fracture	extended	1	No fracture
12	333	12.5	178	not known	extended	1	T8

Table 2 Summary of Peak Acceleration Values at Fracture in the Three Spinal Modes

	Fracture Level (g)	No. of Cadavers	Average Age (yrs)
Extended	17.75 ± 5.55	4	61.5
Erect	10.4 ± 3.79	5	61.0
Flexed	9.0 ± 2.00	3	54.3

Table 3 Student's t Test of Fracture g-Levels Between the Spinal Modes

Modes	Sample Size	t	P
Extended and Erect	9	2.36	0.05
Extended and Flexed	7	2.56	0.05
Erect and Flexed	8	0.58	> 0.05

Table 4 Paired t Test of Strain Data

	Vertebra																	
	AT11			AT12			AL1			AL2			AL4			AL4		
Level	n	t	P	n	t	P	n	t	P	n	t	P	n	t	P	n	t	P
4.5	5	1.63	0.18	7	2.29	0.06	5	3.63	0.02	7	8.03	>.01	5	2.88	0.04	5	3.87	0.02
7.5	-	----	----	-	----	----	-	----	----	3	4.48	0.05	-	----	----	3	6.49	0.02
9.0	3	5.86	0.03	3	19.22	>.01	3	6.97	0.04	3	5.74	0.03	3	3.08	0.09	-	----	----

V. THE EFFECT OF ABDOMINAL PRESSURE

The ability of the abdominal cavity to act as a third load path was investigated. Its role as a load-bearing pressurized cylinder during weight-lifting has been documented by Morris et al (16).

Three male cadavers were subjected to $+G_z$ acceleration in a seated position. A detailed description of the methodology has been given by Prasad et al (17). An intervertebral load cell (IVLC) was positioned in a slotted lumbar vertebral body at either L2 or L3. It measures the load carried by the body and its line of action. A rubber balloon containing a miniature pressure transducer was placed in the eviscerated abdominal cavity. The input pulse was trapezoidal in shape and the peak acceleration ranged from 4 to 9 g. Its duration was about 200 ms. The effect of abdominal pressure on spinal load distribution was studied by making runs with and without pre-pressurization of the balloon. The initial static pressures varied from 6.9 to 20.7 kPa. During the runs, seat acceleration, seat-pan load, intervertebral load and abdominal pressure were measured.

To determine the facet force$^{(RF)}$, the vertical forces acting on the torso at the IVLC level were equated to the inertial force (IF):

$$RB + RF + FB - RM - W = IF \qquad (1)$$

where RB is the measured intervertebral force and the inertial force was taken to be proportional to the seat-pan load. It was reduced by the ratio of the body weight above the IVLC (W), to the total body weight. The abdominal force (FB), was computed as the product of the abdominal pressure and the abdominal cross-sectional area at the level of the IVLC. The abdominal wall reaction (RM), was assumed to be proportional to the abdominal force. The proportionality factor was allowed to vary from 0.15 to 0.50 without affecting the facet force appreciably. A value of 0.3 gave reasonable

estimates of RM which were less than 200 N. The facet force computed from Equation 1 is plotted in Figure 14 along with the intervertebral load. They are for a 9 g run with and without pre-pressurization of 13.8 pKa. The facets initially shared in supporting the inertial load. However, as the head and torso rotated forward, they unloaded and went into tension. The effect of the abdominal load path was to reduce the amount of facet unloading by developing a moment against forward rotation. The intervertebral force was also reduced by this third load path. The results were similar in the runs made on the other two cadavers.

Although abdominal pressure altered the load distribution across the spine, the basic dynamic response described by Prasad et al (17) was not changed. An abdominal pressure of 13.8 pKa (104 mm of Hg) is difficult to generate in 200 ms but an acceleration level of 9 g is less than half of that necessary for pilot ejection. Thus, the effect of abdominal pressure is only of significance at low g levels, and cannot affect the loads sustained by the spine during ejection. The computation of facet force did not account for the balance of angular momentum due to the lack of angular acceleration data for the head and torso. An estimate of RM was made to eliminate the second unknown in Equation 1.

VI. MUSCULAR RESPONSE TO $+G_z$ ACCELERATION

1. Response of the Living System

The biodynamic response of the living spine to $+G_z$ impact acceleration has been studied experimentally by many investigators. They have used a variety of test subjects, including human volunteers, cadavers, and animals, ranging from brown bears to rhesus monkeys. Early work by Geerts (18), Lovelace et al (19), and Stapp (20, 21) was carried out with human volunteers to establish human tolerance limits to $+G_z$ acceleration.

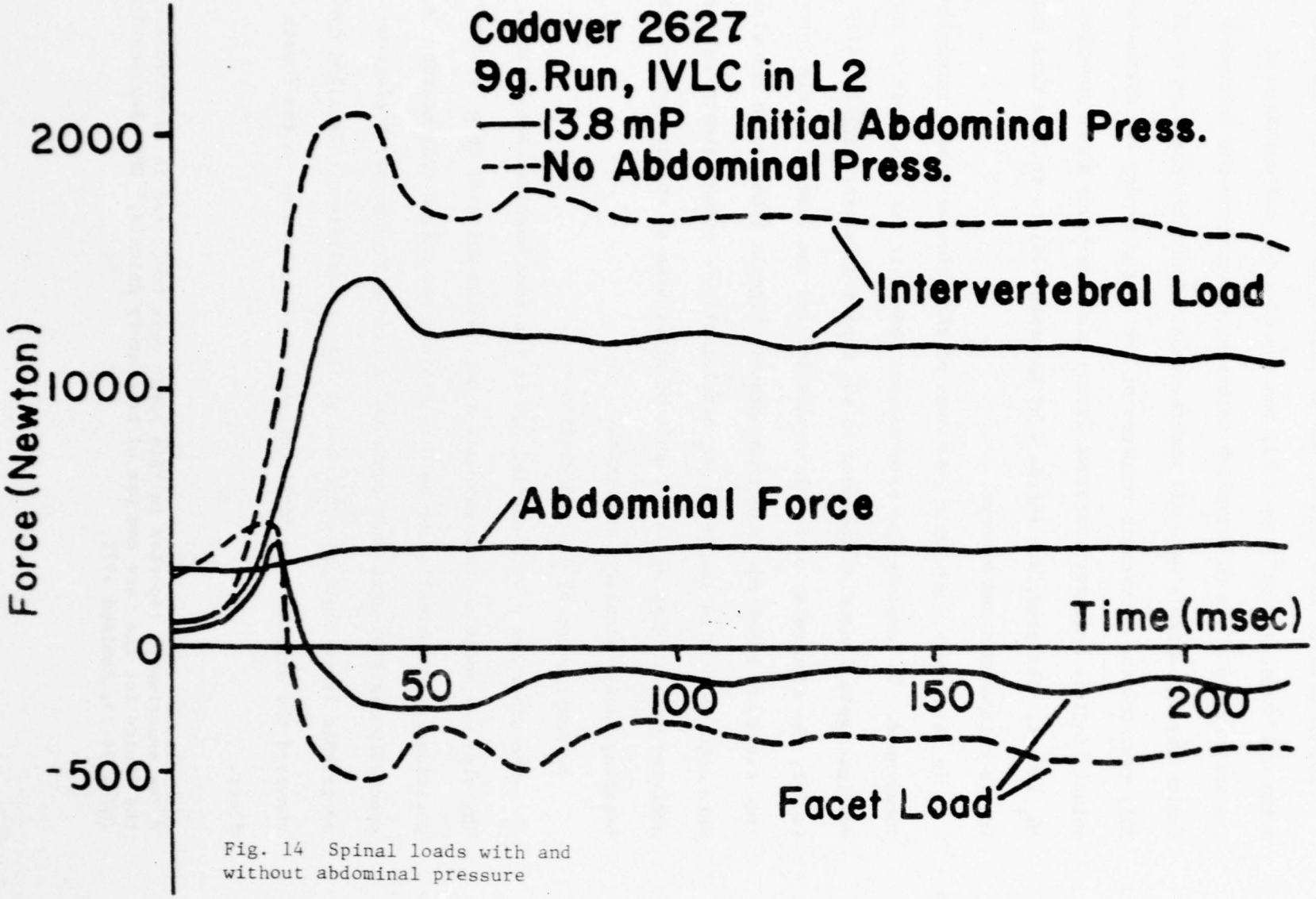

Fig. 14 Spinal loads with and without abdominal pressure

Animal studies were carried out by Beeding and Cook (22), who used swine and bears, and by Stapp (23), who tested swine and chimpanzees. The principal aim was to establish injury patterns above the tolerance limits and the animals were all anesthetized. Recently, Kazarian et al (24, 25), reported the biodynamic response of the rhesus monkey and discussed spinal fracture patterns sustained during high amplitude short duration $+G_z$ impact. The study was extended by Kazarian (26) to include data relating to chimpanzees and baboons.

In this study, cadaveric responses of the spine have been carefully documented. To complete the experimental phase, it was necessary to investigate spinal muscular response to $+G_z$ impact acceleration. In particular, the time delay of muscle activation and the form of muscle force-time curve are reported. Electromyographic signals from canine musculature were acquired during low level $+G_z$ acceleration.* Spinal electromyographic activity was anticipated as a result of stretching of spinal muscles, thus bringing about muscular contraction.

2. Development of Instrumentation

The experiments were carried out in the same vertical accelerator. The sled was modified to accommodate a dog, which was held in a "seated" position by a combination of belt restraints and padded side boards. A specially designed seat back contained a window through which electromyographic leads could be connected to the preamplifiers. Trailing cable conveyed the signals to a data recording station located on the fourth floor.

---

* The experiments reported in this paper were conducted in accordance with the "Guide for the Care and Use of Laboratory Animals," DHEW Publications No. (NIH) 74-23, Revised 1972.

One of the major difficulties in recording noise-free electromyographic signals from an impact sled is the availability of shock resistant on-board amplifiers. They are required to increase the signal-to-noise ratio prior to the transmission of the electromyographic signals through 20 m of trailing cables. Such amplifiers were difficult to obtain commercially and a set of eight was designed and fabricated in the laboratory. As shown in Figure 15, they were packaged within a single case, which could be mounted on the sled. These were differential amplifiers with a variable gain from 0 to about 10,000, and the output was filtered by second order active band pass filters with both low pass and high pass provisions. The amplifier cut off frequencies above 600 Hz, and below 200 Hz, since the frequency content of canine electromyographic signals range from 200 to 400 Hz. The filters and the differential amplification used eliminated most of the noise. The latter feature also permitted freedom of choice in the placing of the electrodes to record only the difference in potential between them. The tendency for the amplifier to become saturated was curbed by placing a I M Ω resistor across the input. The amplifiers were checked out by acquiring electromyographic data from dogs walking on a treadmill. The wire electrodes were inserted in leg muscle groups known to be active during walking. The electrode material and insertion techniques were similar to those developed by Basmajian (27). By visually correlating the oscillograph records with the gait of the dog, it was possible to distinguish the electromyographic signals from noise. From these tests the necessary adjustments and modifications were made to maximize the signal-to-noise ratio.

Needle electrodes inserted at a shallow angle into the muscle were found to be a stable installation. The needle shank was bent 10 to 15 deg-

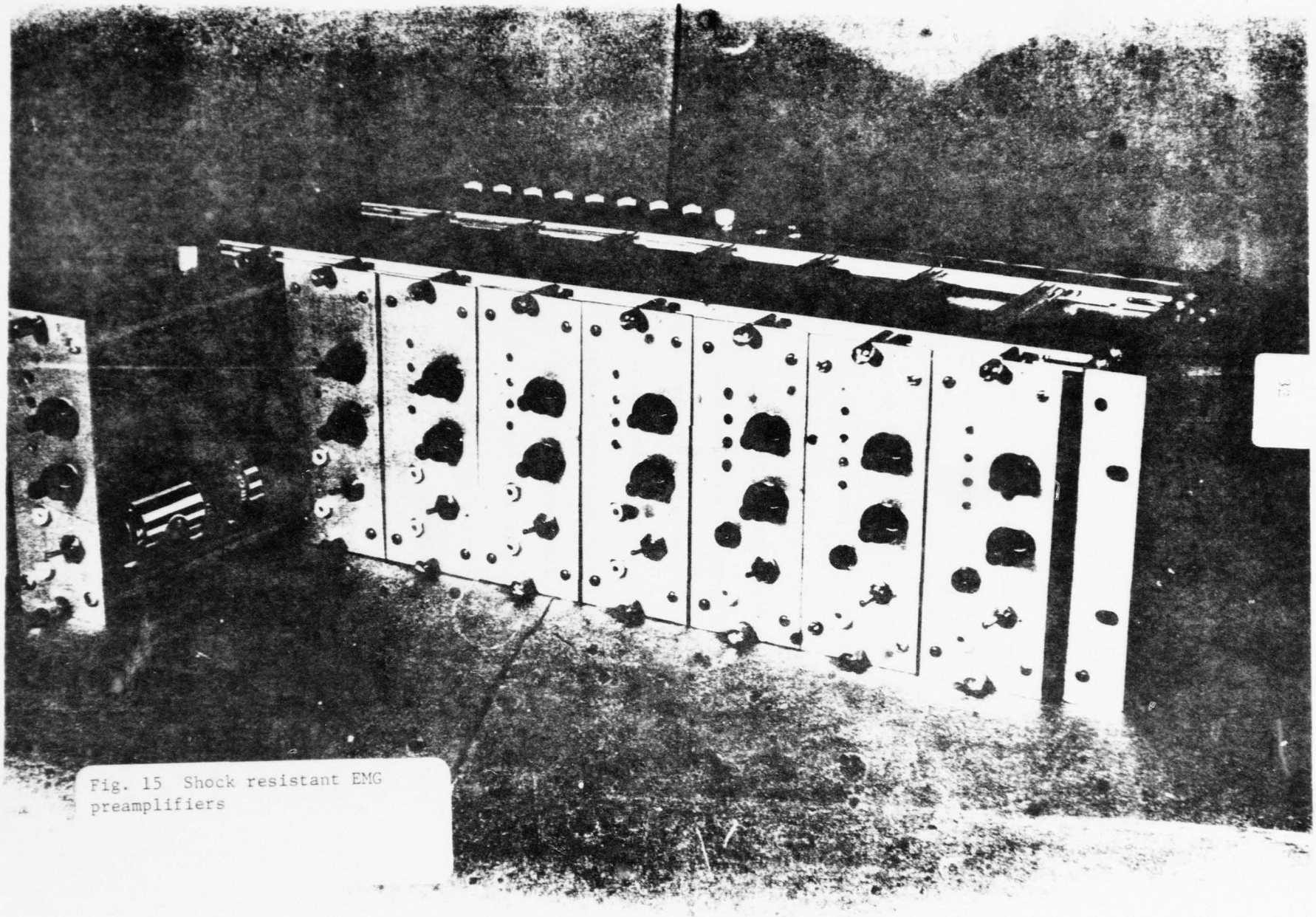

Fig. 15 Shock resistant EMG preamplifiers

rees prior to insertion to permit deeper penetration, and a circumferential groove was machined into the handle of the needle so that it could be securely tied in place by a suture.

The unipolar electrode was selected for the dynamic experiments.* It was 37 mm long and had a tapered stainless steel cannula, with a coaxial insulated nickel-chrome alloy wire exposed at the tip. When compared with a similar bipolar electrode, the signals were of merely identical wave form when isometric contractions of a human flexor carpi radialis muscle were recorded. However, dual monopolar electrodes gave signals that were four times as strong as those from a bipolar electrode.

An excellent shielding and grounding system was required to minimize noise in the minute electromyographic signals. Each electrode was shielded by the needle cannula and a shielded coaxial cable was used for each needle. Ground loops were carefully avoided. For each channel the two active lead cable shields, the body reference ground, and the direct current power supply ground were connected in parallel to the electromyographic preamplifier reference ground. This ground was carried through the trailing cable shield to the common instrumentation ground at the data recording station. All ground and shields were open ended and were carried to a common ground sink.

This impact acceleration experiment had an additional noise problem, which was traced to the whipping of the electrode leads, especially if they struck a rigid surface. Noise levels roughly equivalent to those of the electromyogram were produced. To minimize this noise, several types of miniature coaxial cables were tested. It was determined that type RG-196A/u produced the least noise during the run. It was also essential that each

* Manufactured by Teca Corporation, White Plains, New York 10603.

cable be securely tied down to all surfaces that it could hit.

3. Electrode Sites and Experimental Runs

The muscle groups chosen for electromyographic study were known to be active during flexion and extension movements of the spine. The following groups were monitored:

1. Erector Spinae
   a. Iliocostalis (lumbar)
   b. Longissimus (lumbar, thoracic, and cervical)
   c. Spinalis (thoracic, cervical)
2. Multifudus (lumbar, thoracic)
3. Semispinalis (cervical)

Approximately 24 check-out runs were made to test various components of the experimental system and to develop techniques for acquiring dynamic electromyographic signals. The on-board preamplifiers were subjected to runs at 5 g to verify their structural integrity and to ensure that no spurious signals were generated as a result of the shock loading. There were also several runs designated to eliminate ground loops and other sources of noise. Four runs were then made with the entire electromyography system on board, but the electrodes were not inserted into any muscle; they were kept about 1 cm apart in air. The noise level was found to be low and there were no spurious signals.

A total of 36 runs at 3 and 4 g were made with two additional canine subjects to acquire electromyographic data. They were male beagles weighing approximately 10 kg each. The experimental procedure consisted of setting up the instrumentation to record up to eight channels for electromyography, the sled acceleration, and the seat-pan axial load and sagittal bending moment. Lateral supports were provided in addition to a cross chest belt, and upper torso Y-yoke restraint, and a lap belt.

Upon completion of a series of runs, the dog was given 0.5 ml of Acepromazine and postrun x-ray films were taken to verify needle electrode positions. The animal was also given 1 ml of Floricilin intramuscularly

after the electrodes and sutures were removed.

Figure 16 shows typical electromyographic data from the multifudus lumborum. The input acceleration pulse is superimposed to show the delay in muscle activation. The plot also shows that prior to the run there was very little electromyographic activity.

4. Data Analysis and the Intergrated EMG

The analog data were digitized at a rate of 2000 samples per second per channel, using a PDP-8E minicomputer. The data were prefiltered at a 1000 Hz level to avoid "aliasing" or the generation of false low frequency components. Hannan et al (28) and Viitasalo and Komi (29) have reported sampling rates of 1000 and 1600 per second, respectively. The digitized data were recorded on magnetic tape by an industry-compatible digital recorder so that they could be processed by an IBM 360/67 computer.

"Intergrated" electromyography has long been recognized as a measure of muscle force. The proportionality factor has been difficult to establish except for special cases of isometric contraction or isotonic contraction at a constant velocity. To obtain this force, the electromyographic signal is rectified and a curve smoothing procedure is applied to the rectified data. In this study the rectification was performed by means of a root-mean square (RMS) analysis, based on the frequency content of the signal. For an analog alternating signal, its RMS value is given by,

$$E = \left[(1/T) \int_0^T e^2 dt\right]^{1/2}$$

where E=RMS
e=Instantaneous value
T=Time period of the wave form window

The equivalent digital form is

$$E = \left[(1/N) \sum_{i=1}^{N} e_i^2 dt\right]^{1/2}$$

where N=number of points in the window.

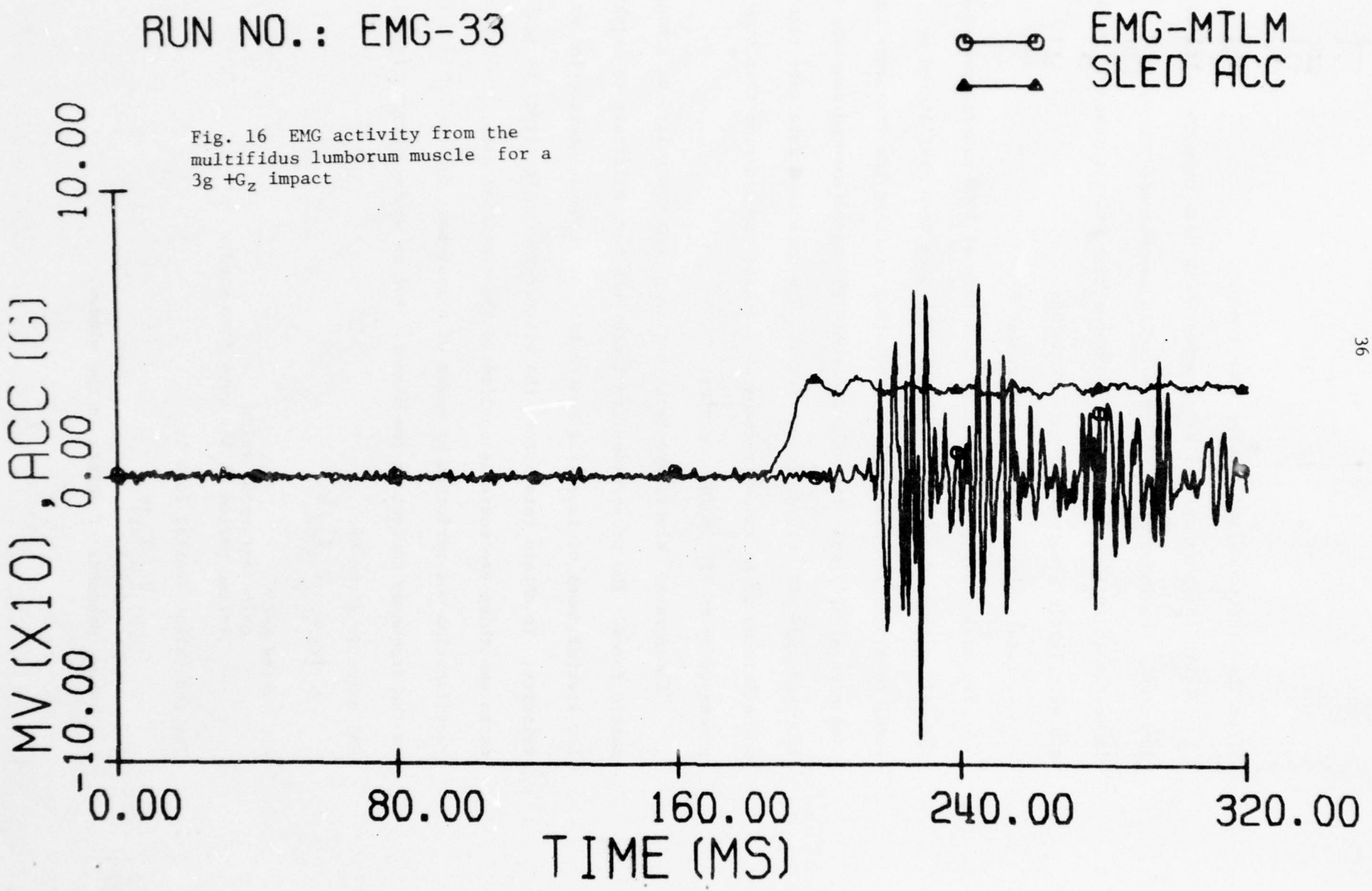

Fig. 16 EMG activity from the multifidus lumborum muscle for a 3g $+G_z$ impact

By using a window size of 5(N=5), the RMS analysis covered at least one fourth of the period of a 100 Hz waveform, since the digitizing rate was 2000 per second. The RMS data were then filtered by the FFT method, with a low pass cut-off frequency of 20 Hz. This ensured that the natural frequency of 8 to 12 Hz for physiological tremor in muscle was preserved. Minimal phase shift resulted from the use of this digital filter.

Figure 17 and 18 are examples of electromyographically derived force for each of the nine muscle sites monitored in the two canine subjects. In general, there was a major burst of electromyographic activity shortly after the onset of acceleration. This initial burst was usually the strongest and resulted in the development of a peak electromyographically derived force. A sustained electromyographic signal and thus a sustained force is shown in Figure 18; these were rather uncommon and appeared to be associated with prerun muscle tone.

In terms of relative magnitudes, the iliocostalis lumborum had the highest peak value, at both 3 g and 5 g. Table 5 lists mean peak values for both dogs at two g levels. On the average, the peak force was higher at 5 g than at 3 g.

Table 5 Peak Values of Electromyographically Derived Force

Muscle Group	Relative Peak Value + S. D. (mv)					
	3 g Runs	(N)	5 g Runs	(N)	All Runs	(N)
Semispin. cap.	4 ± 2.0	(8)	6 ± 4.5	(9)	5 ± 3.6	(17)
Spinalis cerv.	8 ± 9.0	(14)	12 ± 14.2	(15)	10 ± 12.0	(29)
Spinalis thor.	6 ± 4.4	(14)	12 ± 10.1	(15)	9 ± 8.2	(29)
Long. cerv.	8 ± 9.8	(9)	7 ± 7.0	(14)	8 ± 8.0	(23)
Long. thor.	13	(1)	1	(1)	7 ± 8.6	(2)
Long. lum.	4 ± 3.4	(20)	10 ± 11.3	(17)	7 ± 8.4	(37)
Mult. thor.	5 ± 4.8	(9)	6 ± 4.5	(9)	6 ± 4.6	(18)
Mult. lum.	4 ± 2.1	(12)	6 ± 4.0	(15)	5 ± 3.4	(27)
Iliocost. lum.	20 ± 19.3	(2)	15 ± 5.1	(3)	17 ± 10.6	(5)

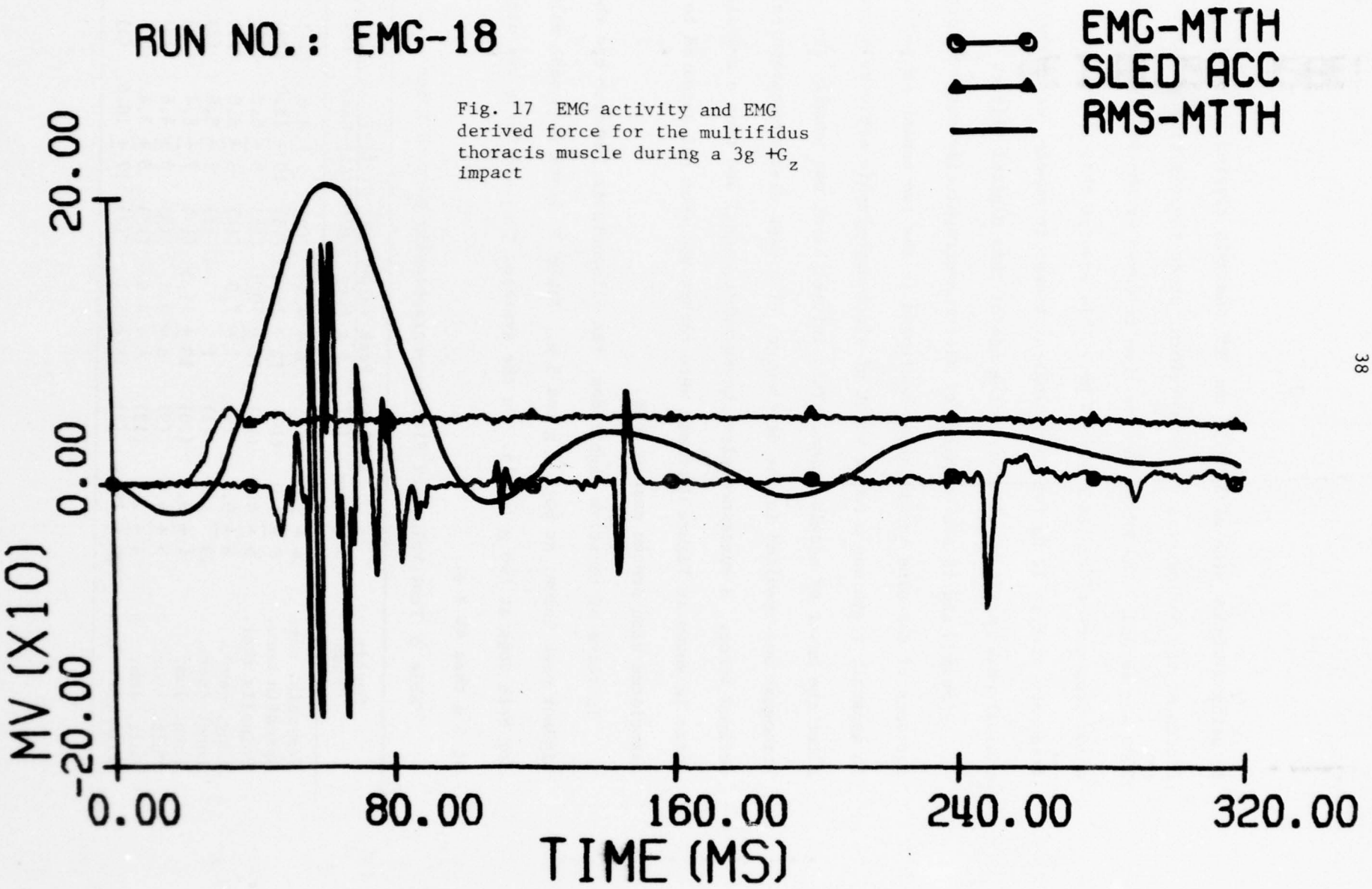

Fig. 17 EMG activity and EMG derived force for the multifidus thoracis muscle during a 3g $+G_z$ impact

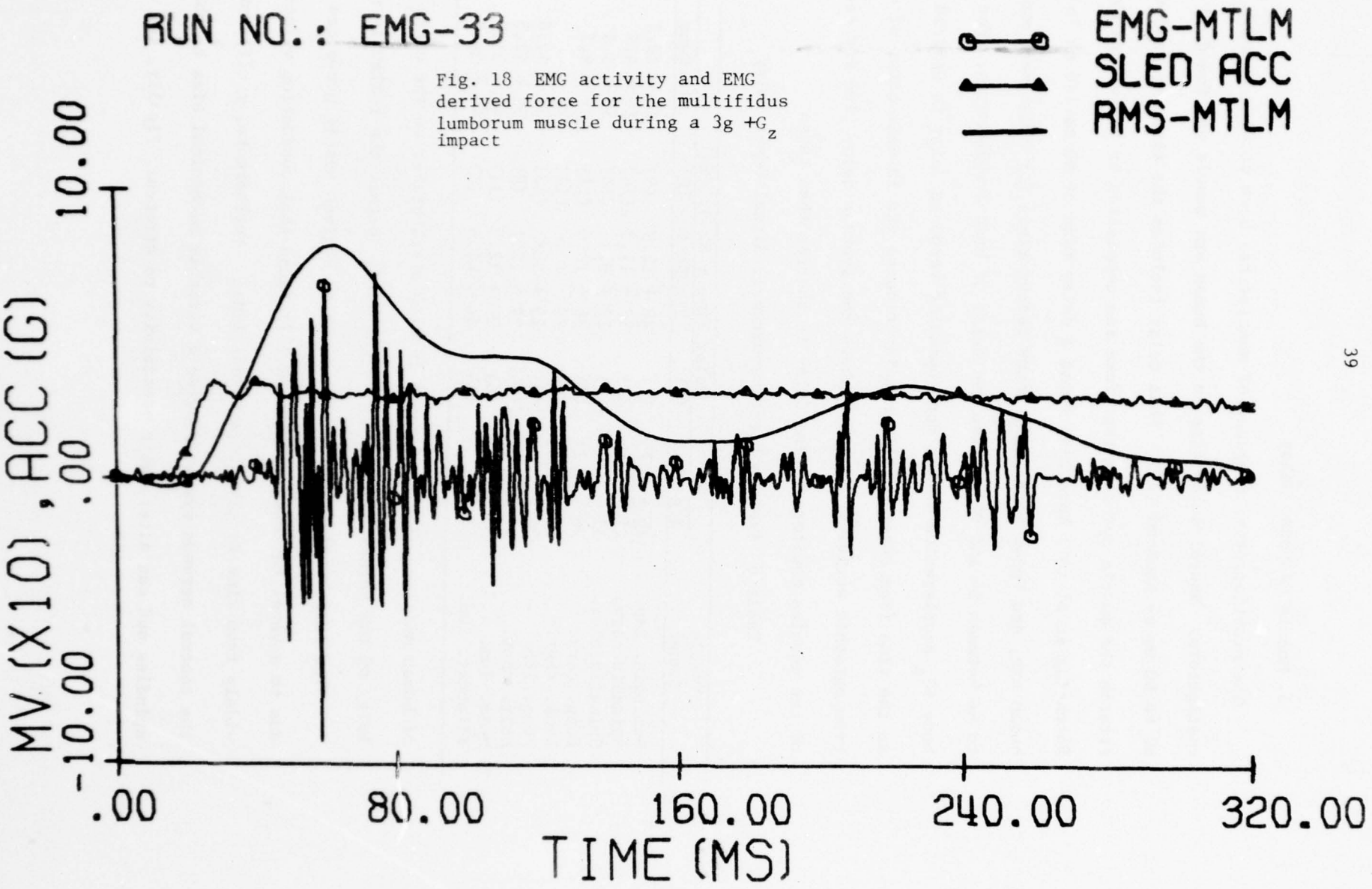

Fig. 18 EMG activity and EMG derived force for the multifidus lumborum muscle during a 3g $+G_z$ impact

5. Muscle Response Delay

The proprioceptive response of muscles has been studied by many investigators. Neural delay time in the human arm muscle was found to be 60 to 80 ms by Hammond (30). This delay includes the time required to stretch the muscle spindles that form the completion of the reflex arc. Soechting et al (31) have also found a delay time of 90 to 140 ms in the human arm, and Foust et al (32) found reflex times for human neck muscles to be between 54 and 92 ms from the onset of head acceleration. For whole body $+G_z$ acceleration in the dog, muscular response delay is defined as the time from onset of sled acceleration to the initial burst of electromyographic activity. Table 6 shows the average delay time for each of the muscles monitored. The delay is shorter than those

Table 6 Average Electromyographic Signal Onset Delay

Muscle Group	Delay Time + S. D. (ms)					
	3 g Runs	(N)	5 g Runs	(N)	All Runs	(N)
Semispin. cap.	25 ± 5.7	(7)	28 ± 12.9	(9)	26 ± 10.2	(16)
Spinalis cerv.	21 ± 6.8	(12)	27 ± 11.3	(14)	24 ± 9.9	(26)
Spinalis thor.	32 ± 8.8	(13)	28 ± 9.2	(14)	30 ± 9.1	(27)
Long. cerv.	26 ± 4.2	(7)	36 ± 10.6	(11)	32 ± 9.7	(18)
Long. thor.	---	(0)	22	(1)	22	(1)
Long. lum.	36 ± 22.3	(18)	25 ± 8.8	(17)	31 ± 17.8	(35)
Mult. thor.	37 ± 11.7	(11)	27 ± 12.1	(8)	32 ± 12.5	(19)
Mult. lum.	58 ± 29.4	(6)	37 ± 12.3	(11)	44 ± 21.7	(17)
Iliocost. lum.	28	(1)	44 ± 41.5	(3)	40 ± 34.9	(4)

of human muscles. The difference is also attributable to the close proximity of the spinal musculature to the cord, so that the reflex is shorter.

The large variation in delay times in a given muscle group can be due to several factors. Basmajian (27) found that conduction velocities varied widely from time to time in any individual. Furthermore, γ efferents from the central nervous system provide a variable mechanical bias to the spindles and can alter their sensitivity to stretch. Finally, the spinal

configuration of the subject can have a significant effect on the response time. Increased kyphosis can shorten the delay in the multifudus thoracis because the curved spine is compressed during $+G_z$ acceleration.

6. Conclusions

The following conclusions were made:

1. Noise-free electromyographic signals were acquired during whole body $+G_z$ impact acceleration, using canine subjects. Nine muscle groups of the spinal musculature were monitored.

2. The validity of the electromyographic data was demonstrated by eliminating possible causes of noise and spurious signals. Small doses of a tranquilizer administered two to two and one-half hours prior to the experimental runs did not affect muscular response.

3. The fast Fourier transform method of spectral analysis was employed to identify electromyographic signals and to filter the root-mean square "intergrated" electromyogram to provide an electromyographically derived force-time curve.

4. The relative peak values of this force were compared for runs at two different g levels. The delay times in muscular response and for the electromyographically derived force to reach a peak value were quantified. The delay in the onset of increased electromyographic activity varied from 21 to 58 ms. These values are somewhat less than those observed in human cervical muscles. The time for the electromyographically derived force to reach its peak ranged from 45 to 135 ms.

VII. A TWO-DIMENSIONAL MATHEMATICAL MODEL

1. Introduction

After Prasad et al (17) reported the existence of two load paths along the spine, one through the vertebral body and the other through the

lamina, via the articular facets, previous models are inadequate in the complete simulation of spinal response. Hence, a two-dimensional discrete parameter model of the spine was formulated to incorporate the two load paths--a factor not considered in any of the existing mathematical models. The objective is to propose a realistic spinal model simulating dynamic response which can be compared to that of an intact spine tested in vivo. Such a model should consider the natural spinal curvatures and the effects of flexion and eccentric inertial loading on the spine. Head and neck motions are simulated and their effects on the forces and moments in the thoracic and lumbar spine can be studies for off-axis impacts in the mid-sagittal plane. The input acceleration pulse can be an arbitrary function of time and the restraint and support systems have been included to properly simulate a seated vehicle occupant. In view of the fact that the experimental data for validation of the model were obtained from cadaveric runs with the spine in the erect and hyperextended mode, the model incorporates the ability to simulate both spinal configurations.

2. Assumptions

The following assumptions were made in the mathematical development:

1. The 24 vertebral bodies, the head and the pelvis are rigid bodies constrained to move in the mid-sagittal plane.

2. Each rigid body has three degrees-of-freedom in the mid-sagittal plane--two translational and one rotational.

3. The intervertebral disks are massless and deformation of the spine takes place at the disks.

4. The disks are replaced by a system of springs and dampers--one spring and damper for axial forces, one spring and damper for shear forces, and another spring and damper arrangement for restoring torques due to re-

lative angular motion between adjacent vertebral bodies.

5. The facets and laminae are springs connected to the vertebral body by a massless rigid rod.

6. Each rigid body is assumed to carry a portion of the torso weight which is eccentric with respect to the centerline of the spine.

7. The rigid bodies are arranged to simulate the spinal curvatures as closely as possible.

3. Equations of Motion

Figure 19 shows the configuration of two successive rigid links that have undergone relative translation and rotation due to deformation of the disk. In the undeformed state, it has been assumed that the axis of any disk is coincident with the axis of the vertebra, that is, the rigid link immediately below it. The position in the mid-sagittal plane of the center of the ith rigid link is determined by the three generalized coordinates, u_i, w_i, θ_i as shown in the figure.

The reaction forces and moments developed on the ith rigid body due to deformation of the ith and the i + 1 disks and the laminae are shown in Figure 20. The changes in the relative angular orientations and the lengths AB, BC, AND A_1A_3 shown in Figure 19 are used to compute the restoring moments, axial and shear forces on the vertebral body and reaction forces at the articular facets. These moments and forces are given by the following equations:

$$T7Y_i = XK_i(AC_i - AC_{0i}) + C_i\dot{AC}_i \tag{2}$$

$$T7X_i = XK_{si}(BC_i - BC_{0i}) + C_{si}\dot{BC}_i \tag{3}$$

$$B_i = XKT_i\{(\theta_i - \theta_{0i}) - (\theta_{i-1} - \theta_{0i-1})\} + C_{ti}(\dot{\theta}_i - \dot{\theta}_{i-1}) \tag{4}$$

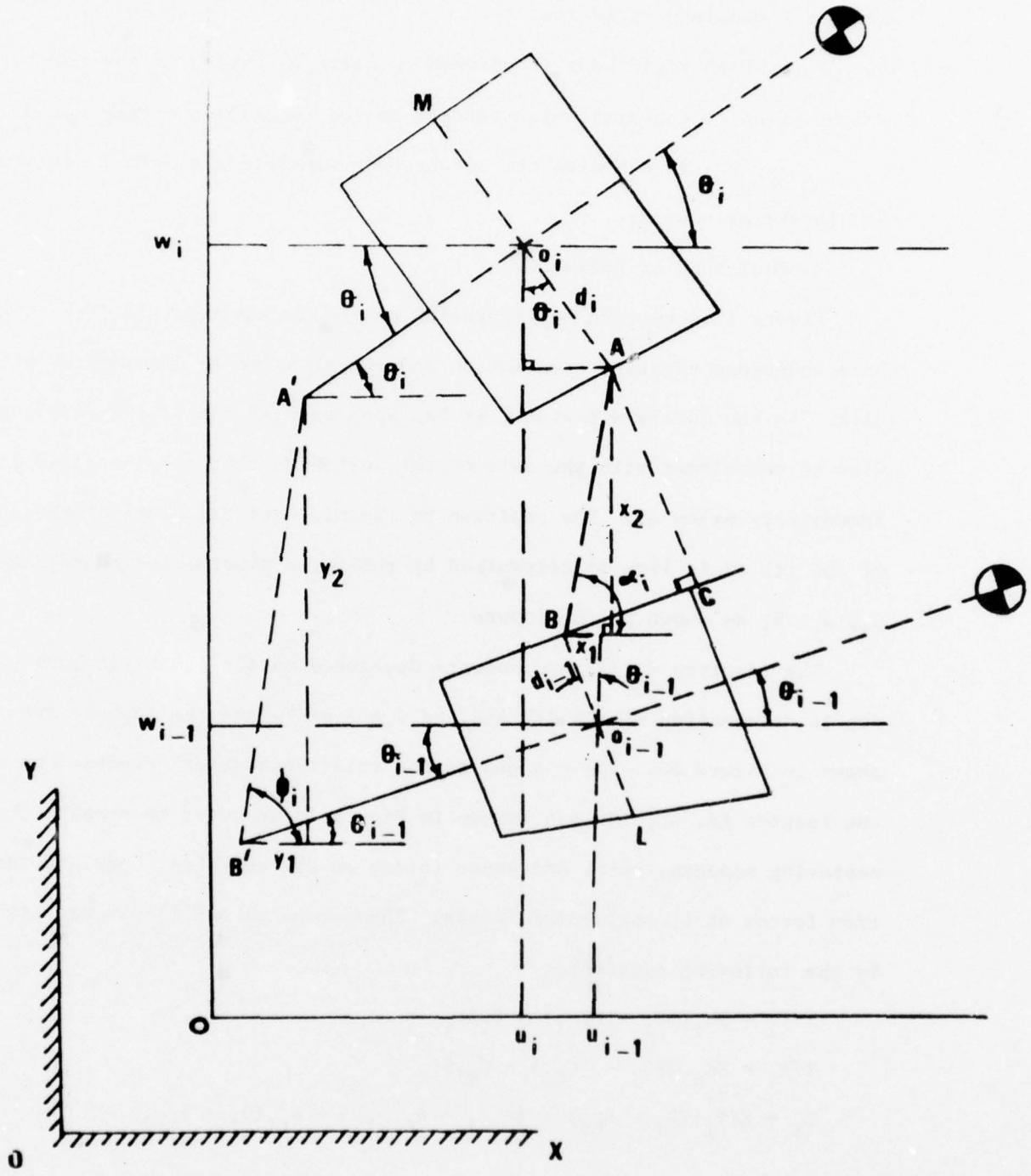

Fig. 19 Configuration of two successive vertebrae

where,

XK_i = stiffness of the axial spring

XK_{si} = stiffness of the shear spring

C_i = damping in axial load

C_{si} = damping in shear loading

XKT_i = stiffness of restoring torque spring

C_{ti} = damping of restoring torque spring

And the subscript "0" denotes the quantity in the undeformed state, at t=0, and (˙) denotes differentiation with respect to time. The forces, $T6Y_i$, $T6X_i$, and the moment B_{i+1} are derived by changing the subscript i on the right side of equations (2)-(4) to i+1.

The articular facets have been modelled by two springs, one limiting rotation and the other limiting the sliding of one vertebra over the adjacent ones. The force resisting relative rotation between the ith and the i-1 vertebrae in the erect mode is given by

$$T51 = XKh_i \cdot h_i \sin \{(\theta_{i-1} - \theta_{0i-1}) - (\theta_i - \theta_{0i})\} \quad (5)$$

where h_i = the distance of the articular facets from the center of the vertebral body and XKh_i = the stiffness of the spring resisting the relative rotation.

In the hyperextended mode, due to the forced change in curvature of the spine, it is assumed that the facets have "bottomed out" and hence the lamina act as another beam parallel to the disk. The change in length A_1A_2 as shown in Figure 19 is used as the measure of axial deformation of this beam, and the force developed is given by

$$T51 = XKh_i \cdot (A_1A_{2i} - A_1A_{20i}) \quad (6)$$

The force resisting sliding motion at the facets between the ith and the i-1 vertebra is given by

$$FX1 = XKh_i \cdot (A_2A_{3i} - A_2A_{30i}) \quad (7)$$

Due to the overlapping nature of the articular facets it is difficult

to define the point of application of the foregoing force. However, in the model, it has been assumed that this force acts perpendicular to the longitudinal axis of the vertebral body at a point $(d_i + AC_i/2)$ below the center of the vertebral body, Figure 20. The reaction of this force on the vertebra immediatly below acts at a distance d_{i-1} above the center of the i-1 vertebra. This assumption is justified because the superior articular facets are shorter than the lamina and the inferior articular facets. As shown in Figure 20 the forces on the ith vertebra parallel to u_i and w_i-axis are

$$\Sigma F_{ui} = (T6Y_i + FX2 - FY1)\cos\theta_i - (T6Y_i + T52 - T51)\sin\theta_i - T7X_i \cos\{\theta_i - (\theta_{0i} - \theta_{0i-1})\} + T7Y_i \sin\{\theta_i - (\theta_{0i} - \theta_{0i-1})\} \quad (8)$$

$$\Sigma F_{ui} = (T6Y_i + T52 - T51)\cos\theta_i + (T6X_i + FX2 - FX1)\sin\theta_i - T7Y_i \cos\{\theta_i - (\theta_{0i} - \theta_{0i-1})\} - T7X_i \sin\{\theta_i - (\theta_{0i} - \theta_{0i-1})\} \quad (9)$$

Taking the sum of moments about the center of gravity.

$$\Sigma M_{Gi} = T7Y_i \cos\{\theta_{0i} - \theta_{0i-1}\}e_i + B_{i+1} - T6Y_i e_i - T6X_i d_i - T7Y_i \sin(\theta_{0i} - \theta_{0i-1})d_i - T7X_i \cos\{\theta_{0i} - \theta_{0i-1}\}d_i - T7X_i \sin\{\theta_{0i} - \theta_{0i-1}\}e_i - B_i + (T51 - T52)(e_i + h_i) - FX2.d_i - FY1(d_i + AC_i/2) \quad (10)$$

There are auxiliary forces and moments which are to be added to these equations whenever applicable. Such loads include the shoulder strap force, lap belt force, seat-back reaction, chin-chest contact forces, and reaction from the hyperextension block.*

Finally, the equations of motion can be written as

$$\Sigma F_{ui} = m_i\{\ddot{X} + \ddot{u}_i - e_i\dot{\theta}_i^2 \cos\theta_i - e_i\ddot{\theta}_i \sin\theta_i\} \quad (11)$$

$$\Sigma F_{ui} = m_i\{\ddot{Y} + \ddot{w}_i + e_i\ddot{\theta}_i \cos\theta_i - e_i\dot{\theta}_i^2 \sin\theta_i\} \quad (12)$$

$$\Sigma M_{Gi} = I_G\ddot{\theta}_i \quad (13)$$

where m_i is the mass supported by the ith body and I_G is the polar moment of inertia about the center of gravity.

Equations (11)-(13) are nonlinear, second order differential equations.

* Details of the auxiliary forces are described by Prasad (33).

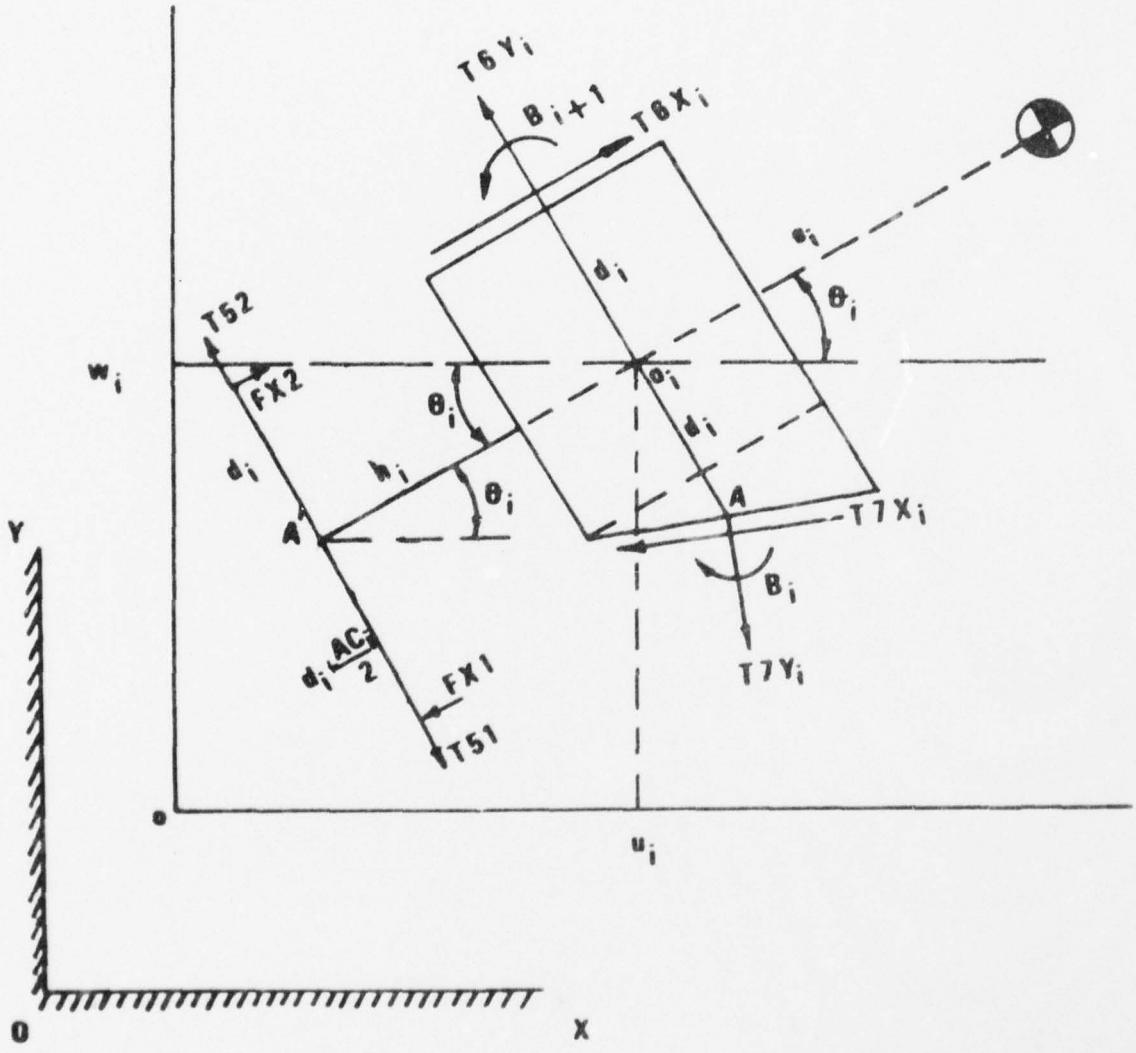

Fig. 20 Free body diagram of the ith vertebra

For each body there are three such equations, hence the total number of equations to be solved simultaneously for i=1-26 is 78. This was achieved by using Hamming's Predictor Corrector method. The accelerations $\ddot{X}$ and $\ddot{Y}$ are input parameters corresponding to the sled acceleration in the x and y directions.

4. Choice of Parameters.

Geometry of the Spine. The model requires the initial coordinates of the center of each vertebral body, the length, the angle the longitudinal axis of the vertebra makes with the vertical, the distance of the articular facets from the center of the vertebral body and the thickness of the disk coincident with each vertebral body. These measurements were made with the help of x-rays taken before each run, with the cadaver placed in the accelerator.

Mass and Moment of Inertia of Each Rigid Link. The model requires the distribution of the mass of the whole body to the rigid links. Liu and Wickstrom (34) have estimated the mass distribution of segmented cadaveric trunks. The mass distribution used in the model is consistent with their data. The three different cadavers used were weighed before the experiment. After the experiments, the torso was cut at the level of L3 and the two halves were weighed again to give the total mass above L3. Three further segments were made of the upper torso--the first consisting of L3 to T8, the second from T8 to C7, and the third from C7 to the head. The three segments were weighed again, their centers of gravity were determined using a load platform which utilizes three load cells at fixed distances from one another. A trifilar pendulum was used to determine the moment of inertia of these segments. Based on the foregoing measured data the mass and moment of inertia at the various vertebral levels were estimated. The mass of the arms was assumed to be distributed to the first five thoracic vertebrae.

Physical Constants. Each rigid link in the model is associated with a disk requiring three-spring constants and facets requiring two spring constants. Hence, a total of 130 spring constants are required for the model. Theoretically, all 130 constants can be different and in an ideal situation, they have to be experimentally determined for each specimen. Very little data are avialable in the literature, and in the case of the articular facets, nothing is available. King and Vulcan (35) have measured the stiffness in compression of the lumbar and the lower thoracic vertebrae. Markolf (36) has measured the axial stiffness of disks from L4 to T8 and has found values ranging from 7000 lb/in. in the lumbar region to 19000 lb/in. in the thoracic region. No data is available for the upper thoracic level. Markolf also gives the rotational stiffness of the disks from 700 in-lb/rad to 2400 in-lb/rad. However, these measurements were made with no preload and at very small deflections. Most biological materials possess a sigmoidal load-deflection characteristic, that is, the stiffness increases with increasing loads. Hence, the foregoing values for rotational stiffness of the disks appear to be much too low; and in the lumbar region, a rotational stiffness of 6000 in-lb/rad was assumed. In the thoracic region, the rib cage imparts more rigidity to the spine, and a rotational stiffness of 12000 in-lb/rad was assumed. In the cervical region, a rotational stiffness of 2400 in-lb/rad was used based on the values given by Vulcan (37). Typical constants used in the model are shown in Table 7.

Table 7 List of Constants Used in Spinal Model (Cadaver 2231)

Segment	Mass (lb-sec^2/in)	Moment of Inertia (lb-in-sec^2)	Linear Disc (lb/in)	Stiffness Facet (lb/in)	Linear Damping Disc (lb-sec/in)	Rotational Stiffness Disc (in-lb/rad)	Rotational Damping Disc (in-lb-sec/rad)
Head	0.19722	0.2816	29991	1200	6.34	2400	2.0
C1	0.01250	0.0013	1595	1200	1.30	2400	1.0
C2	0.01250	0.0013	1595	1200	1.30	2400	1.0
C3	0.00441	0.0016	1595	1200	1.30	2400	1.0
C4	0.00441	0.0025	1595	1200	1.30	2400	1.0
C5	0.00441	0.0030	2537	1200	2.60	2400	1.0
C6	0.00441	0.0030	2537	1200	2.60	2400	1.0
C7	0.00441	0.0040	2537	1200	2.60	2400	1.0
T1	0.00441	0.0066	16562	2000	25.00	12000	20.0
T2	0.01031	0.0184	16562	2000	25.00	12000	20.0
T3	0.01031	0.0255	16562	2000	25.00	12000	20.0
T4	0.01031	0.0273	26562	2000	25.00	12000	20.0
T5	0.01031	0.0340	16562	2000	25.00	12000	20.0
T6	0.01656	0.0392	10310	2000	20.00	12000	20.0
T7	0.01656	0.0476	10310	2000	20.00	12000	20.0
T8	0.01656	0.0491	10310	2000	15.00	12000	20.0
T9	0.01656	0.0546	10310	2000	15.00	12000	20.0
T10	0.01656	0.0534	8000	2000	15.00	12000	20.0
T11	0.00254	0.0625	8000	2000	10.00	6000	10.0
T12	0.00254	0.0156	8000	2000	10.00	6000	10.0
L1	0.00254	0.0156	8000	6000	10.00	6000	10.0
L2	0.00160	0.0156	8000	6000	10.00	6000	10.0
L3	0.00160	0.0156	8000	6000	10.00	6000	10.0
L4	0.00160	0.0700	8000	6000	10.00	6000	10.0
L5	0.00160	0.0700	8000	6000	10.00	6000	10.0
Pelvis	0.02991	0.4540	10000	0	240.00	0	20.0

Stiffness and damping values refer to the disc or facet below the segment

5. Model Validation

Experiments involving the use of human cadavers were carried out to validate this model. In both the computer and experimental simulations, the conditions at both ends of the spinal column are specified. An acceleration input is applied at the pelvis while the top of head is to remain stress-free at all times. Kinematic and/or kinetic quantities can be measured anywhere along the column for comparison with those predicted by the model. The parameter used for validation in this case is the force between two

adjacent vertebral bodies. An intervertebral body load cell (IVLC) was developed to provide the magnitude and the line of action of this force. The experimental techniques and instrumentation used have been described in detail by Prasad et al (38). However, it should be pointed out that the IVLC was instrumental in the establishment of the role of the articular facets and the posterior spinal structures. Facet loads were obtained by first computing the total spine load at the level of the IVLC. It was taken to be the product of the measured seat-pan load and the ratio of the torso weight above the IVLC to the total body weight. The difference between the total spine load and the intervertebral load is the facet load. Strain gages installed on the posterior surface of the lamina provided additional qualitative evidence of the facet load. As shown in Figure 12 the facet load curve is mirrored by that of the posterior strain gage, including the instant of time at which a change in sign occured.

Three cadavers were subjected to $+G_z$ or seat-to-head trapezoidal acceleration pulses of 6, 8, and 10 g, in the erect and hyperextended mode. The rate of onset was approximately 250 g/sec. Figures 21-24 show comparisons for each of the three cadavers at different g levels and spinal configurations.* A comparison of both the intervertbral load and the facet load for Cadaver 2231 is shown in Figure 21. This run was made at 10 g in the erect mode. These loads were measured at the level of L2-L3. Note the change in sign of the facet load as a result of the eccentricity of the head and torso with respect to the spine. In both the model output and the experimental data, the second intervertebral force peak coincides with the maximum tension in the facets. Figure 22 shows a run in the hyperextended mode using the same cadaver and the same g level. There is a marked

* Comparison for all 18 runs are given by Prasad (33).

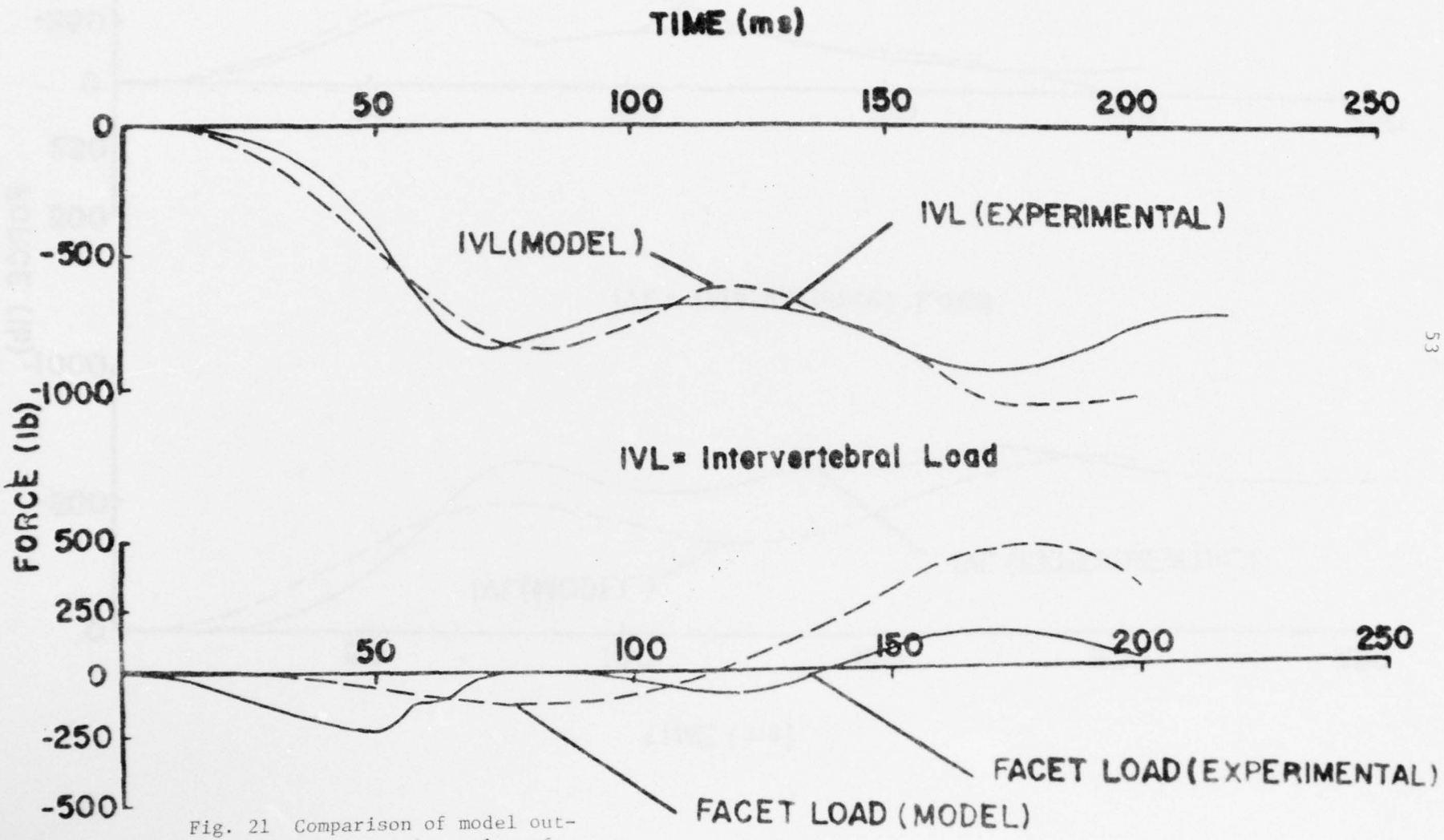

Fig. 21 Comparison of model output and experimental results of a 10g run on Cadaver 2231 in the erect mode

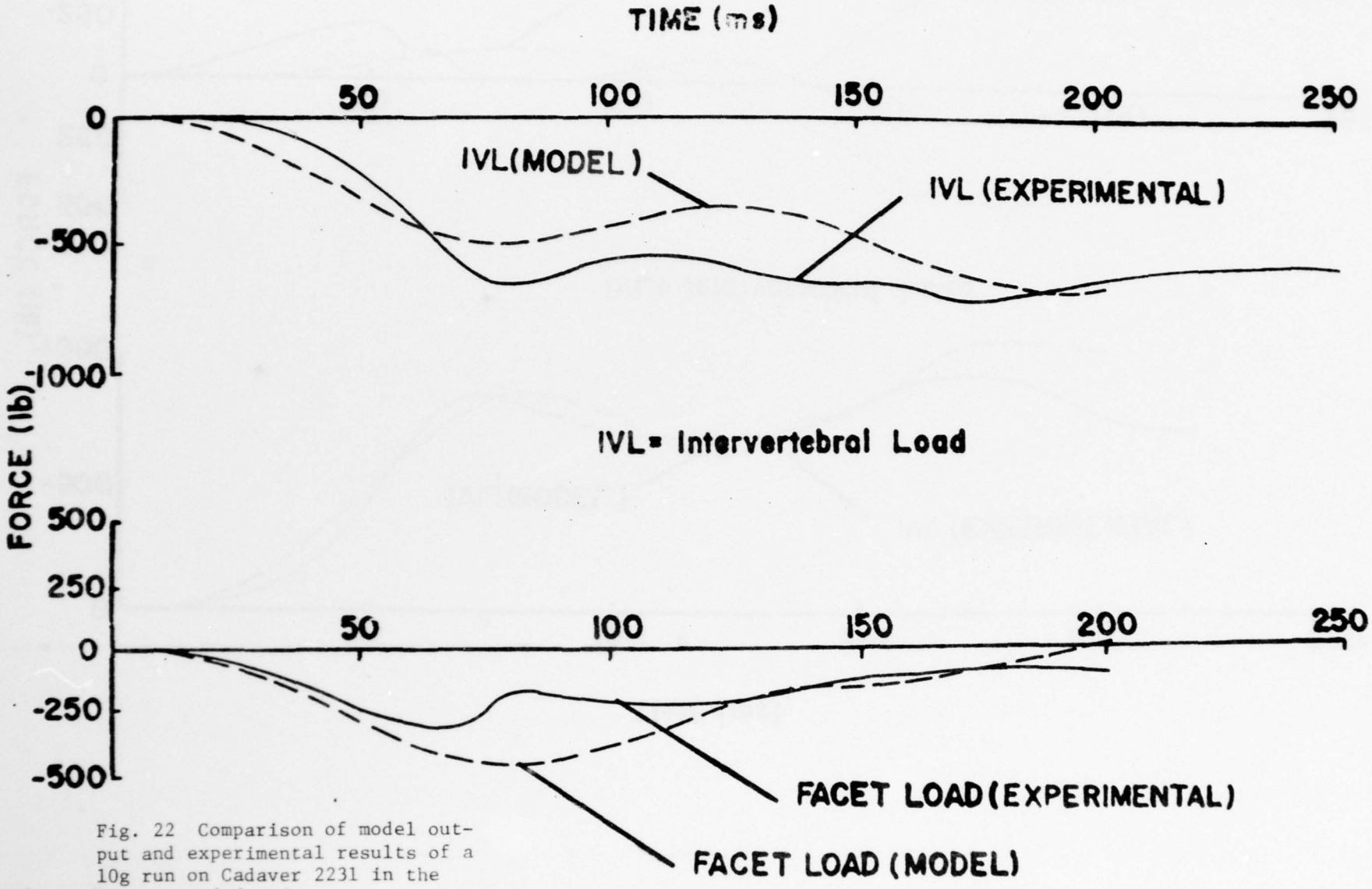

Fig. 22 Comparison of model output and experimental results of a 10g run on Cadaver 2231 in the hyperextended mode

reduction in intervertebral load accompanied by an increase in compression at the facets which did not go into tension or unload as before. The model predicted this phenomenon and offers an explanation for the dramatic increase in fracture g level reported by Ewing et al (4). It is interesting to note that there was an increase of only 110 N in the peak intervertebral load when the g level was increased from 8-10 g. The change was 1156 N for a similar increase from 6-8 g. The model predicted a change of 334 N for the first case and 1121 N for the second.

A 6 g run on Cadaver 2209 is shown in Figure 23. This is a comparison of a run made in the erect mode. Again, there was unloading of the facets.

A hyperextended run at 8 g on Cadaver 2413 is shown in Figure 24. Although the peak values of the intervertebral loads matched, the choice of the model constants resulted in a system with a higher natural frequency than that of the cadaver. The facets barely went into tension towards the end of the pulse and the model was able to predict this.

6. Discussion and Conclusions

A mathematical model of the spine has been formulated to simulate its response to impact acceleration in the sagittal plane. It has been validated by comparing its predictions with experimental data derived from 18 runs on 3 cadavers which were subjected to 3 levels of $+G_z$ acceleration. The question of what constitutes proper validation of a model cannot be fully answered. However, some basic ground rules were established for this validation procedure. Since the acceleration levels were relatively low and the differences were small, it was decided that there was to be only one set of constants for each cadaver for all 6 runs. Variation among cadavers was permitted since it is well known that biological differences are quite large. However, the values of these constants must not deviate too far

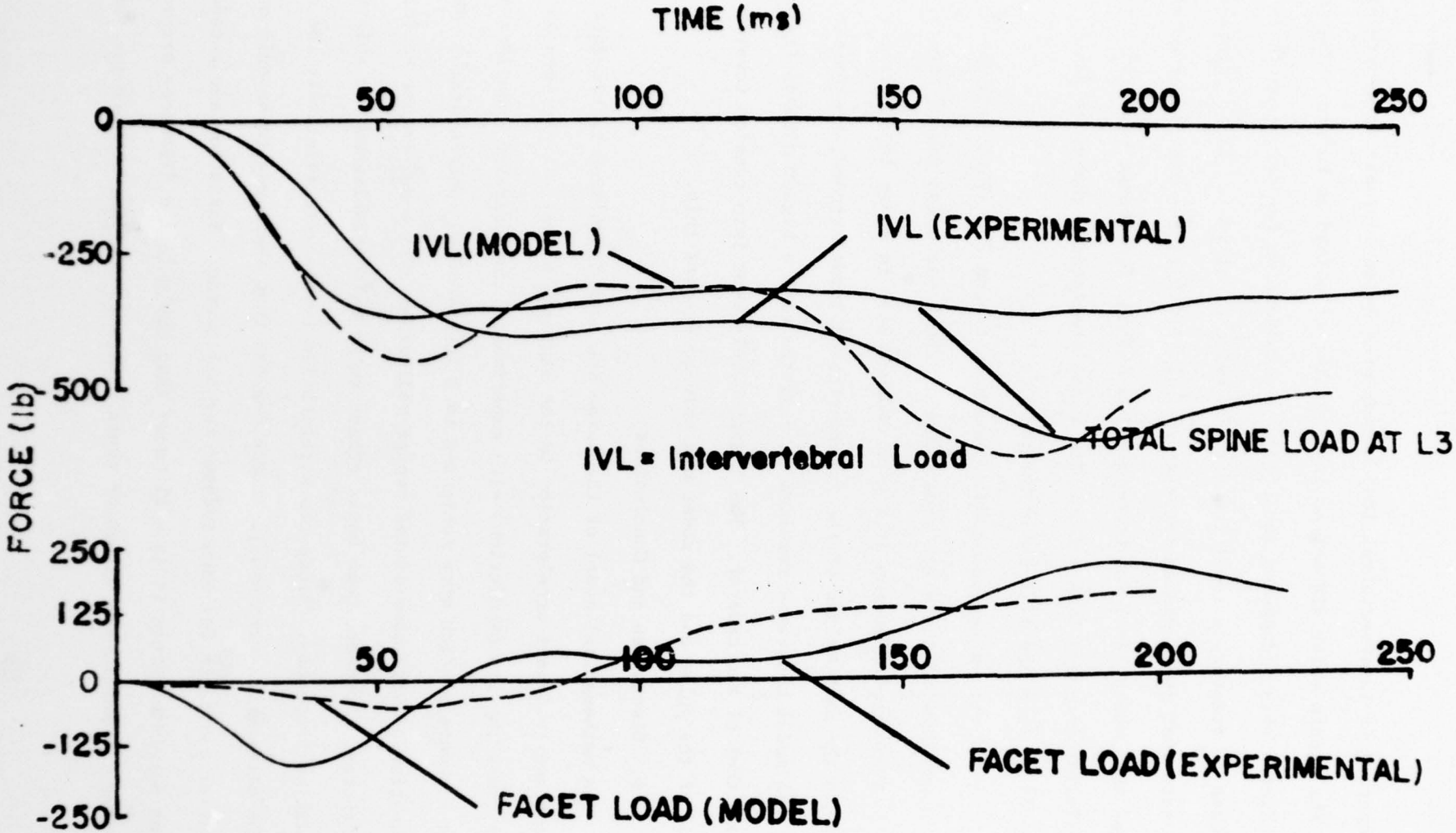

Fig. 23 Comparison of model output and experimental results of a 6g run on Cadaver 2209 in the erect mode

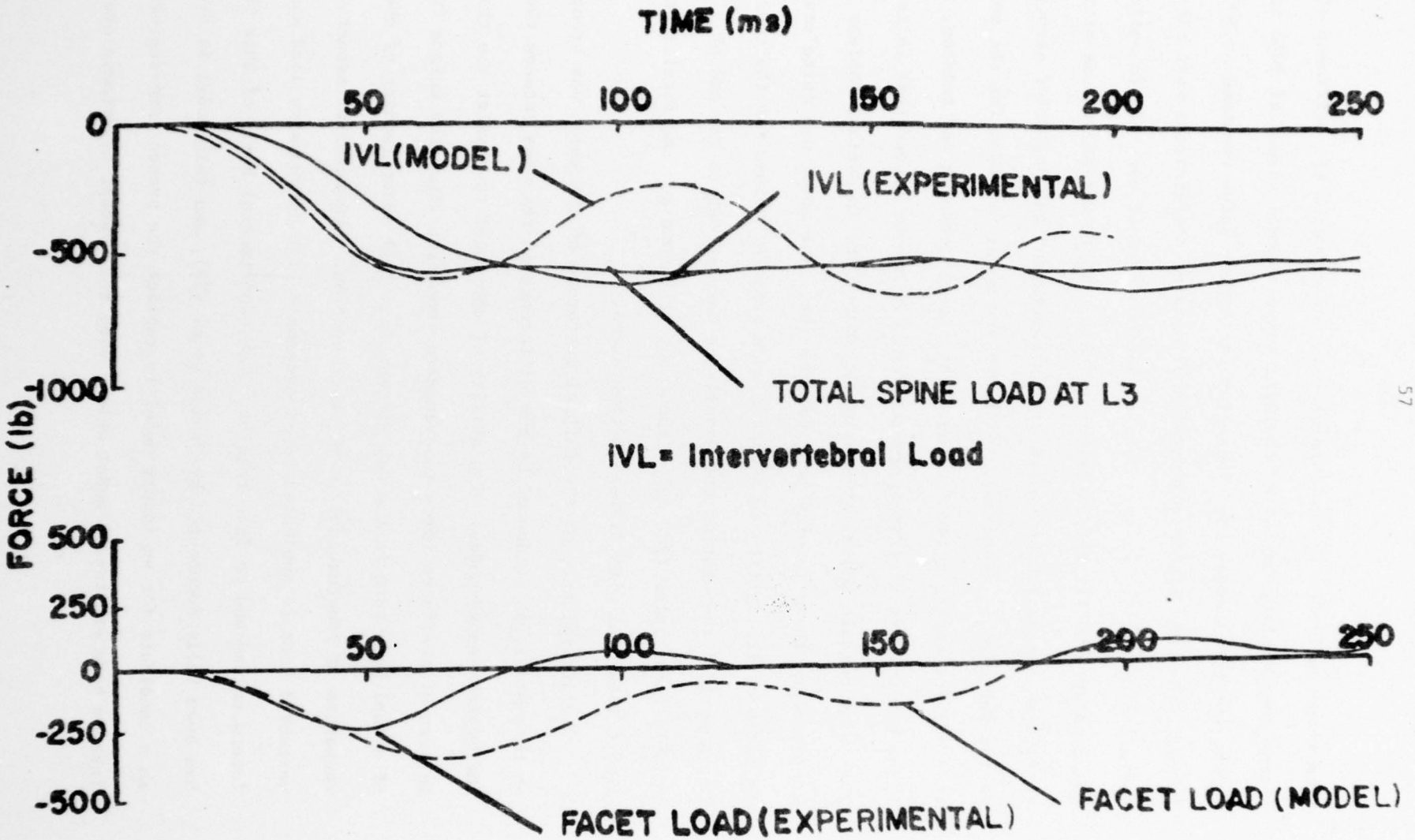

Fig. 24 Comparison of model output and experimental results of an 8g run on Cadaver 2413 in the hyperextended mode

from those published in the literature. For example, the stiffness of the spring representing the lower thoracic spine assumed values of 8000 to 10000 lb/in. for the 3 cadavers. Those for the lumbar spine remained at 8000 lb/in. In fact, the same linear and rotational damping coefficients were also used for all 3 cadavers. In any case, no serious attempt was made to optimize the constants to fit the experimental data. There was an extreme paucity of data as far as the stiffness of the facets and the posterior structures of the vertebra is concerned. Although the model provides for the selection of different spring rates for the facets in compression and tension, the same value was used as a first approximation. It can be argued that in tension the joint capsule and all posterior ligaments are in action, whereas in compression, there is only bony deformation. The model was quite stable in terms of its ability to accept a wide range of values for the constants. The numerical computation can usually be carried out to the end of a reasonable input pulse (200 ms) without any breakdown and the results are almost identical with different time steps.

The significance of the initial curvature of the spine was brought out by this model, as evidenced by the difference in response between the erect and hyperextended modes. The ability of the model to predict the change in sign of the facet force is even more important since the unique feature of a dual load path is the key element in a full understanding of the mechanism of fracture due to $+G_z$ acceleration. The anterior aspect of the vertebral body is subjected to an extremely high compressive load when the facets unload and go into tension. The experimental basis of this phenomenon has been fully documented by Prasad et al (38), and this model is proposed as a candidate for an injury model to replace the present one-degree-of-freedom base excitation model which uses the concept of dynamic overshoot

as a measure of peak load on the spine. In fact, there is very little dynamic overshoot in the cadaver data acquired thus far. The first peak in the intervertebral load is invariably lower than the second for a run made in the erect mode. That is, the peak load experienced by the vertebral bodies occurs much later in the pulse and is a result of head and torso kinematics and load transfer. It is not the result of a dynamic overshoot.

VIII. MECHANISM OF INJURY AND INJURY PREDICTION

On the basis of the data obtained, it is now possible to assemble the research results on spinal injury and propose an injury mechanism that fully explains the commonly observed anterior wedge fractures sustained by pilots during emergency egress. Previous work by Vulcan and King (39) established the fact that during caudocephalad ($+G_z$) acceleration, the spine is subjected to both axial compression and bending. The bending effects are due to the eccentricity of the torso with respect to the spine and are enhanced by the forward rotation of the head and torso. Subsequent work by Ewing et al (4) showed that fracture levels could be raised significantly by placing a 5.7 cm thick hyperextension block opposite L1 on the seat back. The curvature of the spine was altered by the block, but there was insufficient movement to decrease the eccentricity of the torso and, hence, the bending moment on the spine. Nevertheless, the average level of fracture was raised from 10 to 18 g, and the decrease in anterior strains was generally significant at the 95 percent confidence level. The hypothesis that the facets act as motion limiters led to this documentation of their role during $+G_z$ acceleration. In the erect spinal mode the facets tend to unload and go into tension, causing the vertebral bodies to sustain more compressive load than the total spine load. This occurs when the head and torso undergo maximal forward flexion. The anterior wedge fractures

are therefore the result of eccentric compression coupled with the unloading of the facets. In the hyperextended mode the facets relieve the vertebral bodies of some of the compressive load, and thus it was possible to raise the fracture level by such a considerable margin.

The model output can be used to predict the forces and moments sustained by each vertebra at each instant of time. The intervertebral axial force is plotted as a function of distance above the seat pan in Figure 25 for a 10 g run. The curves are plotted for instants of time at which the first and second peaks occur and for both the erect and hyperextended mode. Note that the intervertebral load is less in the hyperextended case than that for the erect mode. Also the lower thoracic spine sustains a proportionally higher load and is therefore more susceptible to fracture. These runs simulate the cadaver runs carried out on the vertical accelerator, and since the cadavers were eviscerated for the installation of strain gages and the intervertebral load cell, the inertial load on the lumbar spine was minimal. By use of the mass distribution data provided by Liu and Wickstrom (34), it was found that the lumbar spine sustained a slightly higher load at both the first and second peaks.

If the dynamic fracture load for vertebrae is known, this model can be used as an injury predictor. The fracture loads can be plotted as a band on Figure 25, and injury is likely if the force sustained by any vertebra exceeds its fracture level as a conservative estimate, the static fracture loads given by Ruff (7), can be used as a limit, pending the acquisition of dynamic data.

IX. CONCLUSIONS

Sufficient data are now available to formulate a comprehensive mechanism of injury to the spine. A mathematical model has been developed and validated. It can be used to further the understanding of this mechanism and

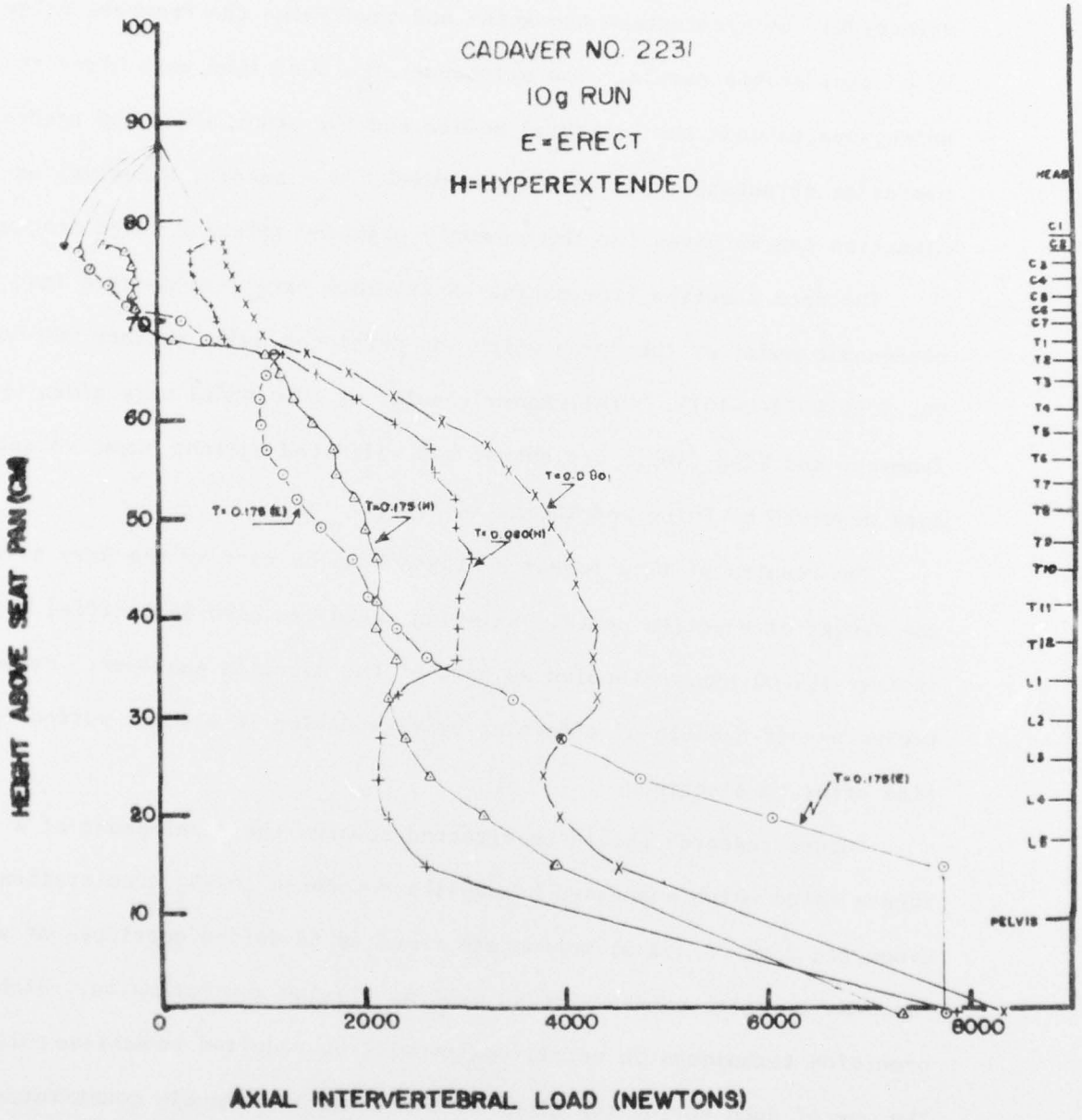

Fig. 25 Intervertebral axial loads along the spine for a 10g run

to predict injury as a result of an arbitrary input pulse. Since the mechanism is not one of simple compressive failure, it was found that the restraint system presently available in military aircraft can be used effectively to hyperextend the spine and thus raise the fracture g level by a considerable margin. The existence of a dual load path along the spine, one through the vertebral bodies and the other along the facets, and posterior structures, has been documented. As a result, a logical explanation can be given for the commonly observed anterior wedge fractures.

The data acquired from canine experiments were incorporated into a biodynamic model of the spine which was developed under another ONR Contract No. N00014-75-C-1015. Preliminary results of this model were given by Tennyson and King (40). Its output was validated against human volunteer data acquired by Ewing and Thomas (41).

The results of this research program can be used by the Navy to improve the design of ejection seats. Existing seats can also be modified to include spinal hyperextension as part of the ejection sequence. Present technology is capable of effecting hyperextension in a short period of time prior to ejection.

Future research should be directed towards the development of a surrogate spine which possesses human-like responses to $+G_z$ acceleration. Kinematic data of spinal motion are required to define corridors of spinal response to axial compression as well as flexion and extension. High precision techniques in accelerometry will be required to achieve this end. The use of such surrogates along with mathematical models constitutes an ideal approach to the design of safe ejection seats of the future.

X REFERENCES

1. Latham, F.: A study in body ballistics: seat ejection. Proc. R. Soc. (B), 147:121-139, 1957.

2. Hess, J. L and Lombard, C. F.: Theoretical investigations of dynamic response of man to high vertical accelerations. Aviation Medicine, 29:66-75, 1958.

3. King. A. I., Vulcan, A. P. and Cheng, L. K.: Effects of bending on the vertebral column of the seated human during caudocephalad acceleration. Proc. 21st ACEMB, p. 32.3, 1968.

4. Ewing, C. L., King, A. I. and Prasad, P.: Structural considerations of the human vertebral column under $+G_z$ impact acceleration. J. of Aircraft, 9(1):84-90, 1972.

5. Ewing, C. L.: Non-Fatal Ejection Vertebral Fracture, U.S. Navy, Fiscal Years 1959 through 1965: Costs. Aerospace Medicine.

6. Patrick, L. M.: Caudocephald static and dynamic injuries. Proc. of the 5th Stapp Car Crash Conf., edited by M. K. Cragun, Univ. of Minnesota, Minneapolis, Minn., pp. 171-181, 1962.

7. Ruff, S.: Brief acceleration: less than one second. German Aviation Medicine World War II, Vol. 1, U.S. Government Printing Office, Washington, D.C., pp. 584-594, 1950.

8. McElhaney, J. and Roberts, V.: Mechanical properties of cancellous bone. AIAA paper 71-111, New York, 1971.

9. Gray, H.: Anatomy of the Human Body. Goss, C. M., ed., 25th ed., Lea and Febiger, Philadelphia, Pa, pp. 75-76, 1948.

10. Basmajian, J. V.: Primary Anatomy, 6th ed., The Williams and Wilkins Co., Baltimore, Md., p. 27, 1970.

11. Fick, R.: Handbuch der Anatomie und Mechanik der Gelenke. Ver lag Gustav Fischer, Jena, 1904.

12. Basmajian, J. V.: Grant's Method of Anatomy, 8th ed., The Williams and Wilkins Co., Baltimore, MD., p. 18, 1971.

13. Strasser, H.: Lehrbuch d. Muskel und Gelenkmechanik. J. Springer, Berlin, 1913.

14. Nachemson, A.: Lumbar intradiscal pressure. Acta Orthop. Scand. Suppl., Vol. 43(1), 1960.

15. Nachemson, A.: The influence of spinal movements on the lumbar intradiscal pressure and on the tensile stress in the annulus fibrosus. Acta Orthop. Scand., 33:183, 1963.

16. Morris, J. M., Lucas, D. B., and Bresler, B.: The role of the trunk in the stability of the spine. Report No. 42, Biomechanics Laboratory, Univ. of Calif., San Francisco, Ca., 1961.

17. Prasad, P., King, A. I., Ewing, C. L.: The Role of Articular Facets During $+G_z$ Acceleration. ASME Paper No. 73-WA/Bio-31, 1973.

18. Geertz, A.: Grenzen und sonderprobleme bei der amwendung von sitnkatapulten (limits and special problems in the use of seat catapults). Translation No. U-10-46-22. AAF Aeromedical Center, 1946.

19. Lovelace, W. R., Baldes, E. and Wulff, V. J.: The ejection seat for emergency escape from high-speed aircraft. ASTIA ATI-7245, 1946.

20. Stapp, J. P.: Human and chimpanzee tolerance to linear decelerative force. Paper presented at Conference on Problems of Emergency Escape in High-Speed Flight, Wright-Patterson Air Force Base, Ohio, 1952.

21. Stapp, J. P.: Tolerance to abrupt deceleration. Collected Papers on Aviation Medicine, AGARDograph No. 6, London, Butterworth Scientific Publications, pp. 122-169, 1955.

22. Beeding, E. L., Jr., and Cook, J. E.: Correlation tests of animals and humans. Proceedings of the 5th Stapp Automotive Crash Conference. Minneapolis, University of Minnesota, pp. 125-132, 1962.

23. Stapp, J. P., Effect of mechanical force on living tissues. I. Abrupt deceleration and wind blast, J. Aviation Med., 26(4):268-288, 1956.

24. Kazarian, L. E., Boyd, D. D., and von Gierke, H. E.: The dynamic biomechanical nature of spinal fractures and articular facet derangement. AGARD Conference Proceedings No. 88 on Linear Acceleration of Impact Type, NATO, AGARD-CP-88-71, Paper No. 19, 1971.

25. Kazarian, L. E., Hahn, J. W., and von Gierke, H. E.: Biomechanics of the vertebral column and internal organ response to seated spinal impact in the rhesus monkey (macaca mulatta). Proceedings of the 14th Stapp Car Crash Conference. New York, Society of Automotive Engineers, pp. 121-143, 1970.

26. Kazarian, L. E.: The primate as a model for crash injury. Proceedings of the 19th Stapp Car Crash Conference. Society of Automotive Engineers, Warrendale, pp. 931-963, 1975.

27. Basmajian, J. V.: Muscles Alive, The Williams & Wilkins Co., Baltimore, 1967.

28. Hannan, A. G., Inkster, W. C. and Scott, J. D.: Peak EMG activity and Jaw closing force in man. J. Dent. Res. 54(3):694, 1975.

29. Viitasalo, J. H. T., and Komi, P. V.: Signal characteristics of EMG with special reference to reproducibility of measurements. Acta Physiol. Scand., 93:531-539, 1975.

30. Hammond, P. H.: An experimental study of servo action in human muscular control. Third International Conference on Medical Electronics, p. 190, 1960.

31. Soechting, J. F., Stewart, P. A. Hawley, R. H., Paslay, P. R. and Duffy, J.: Evaluation of neuromuscular parameters describing human reflex motion. J. Dynamical Systems, Measurement, and Control. Trans., ASME, 93:221-2. , 1971.

32. Foust, D. R., Chaffin, D. B., Snyder, R. G. and Baum, J. K.: Cervical range of motion and dynamic response and strength of cervical muscles. Proceedings of the 17th Stapp Car Crash Conference, Society of Automotive Engineers, New York, pp. 285-308, 1973.

33. Prasad, P.: The dynamic response of the spine during +G_z acceleration. Ph.D. dissertation, Wayne State University, Detroit, 1973.

34. Liu, Y. K., and Wickstrom, J. K.: Estimation of the inertial property distribution of the human torso from segmented cadaver data. Perspectives in Biomedical Engineering, ed., Kenedi, R. M., University Park Press, Baltimore, pp. 203-213, 1973.

35. King, A. I. and Vulcan, A. P.: Elastic deformation characteristics of the spine. J. of Biomechanics 4:413-429, 1971.

36. Markolf, K. L.: Stiffness and damping characteristics of the thoraco-lumbar spine. Proceedings of Workshop on Bioengineering Approaches to Problems of the Spine, publ. by Div. of Research Grants NIH, Bethesda, pp. 87-143, 1970.

37. Vulcan, A. P.: Response of the lower vertebral column to caudocephalad acceleration. Ph.D. dissertation, Wayne State University, Detroit, 1969.

38. Prasad, P., King, A. I. and Ewing, C. L.: The role of articular facets during +G_z acceleration. J. of Applied Mechanics, 41(2), Trans. ASME, Vol. 96, Series E., June 1974.

39. Vulcan, A. P. and King, A. I.: Forces and moments sustained by the lower vertebral column of a seated human during seat-to-head acceleration. Dynamic Response of Biomechanical Systems, N. Perrone, ed., American Society of Mechanical Engineers, New York, pp. 84-100, 1968.

40. Tennyson, S. A. and King, A. I.: A biodynamic model of the human spinal column. Paper No. 760771, In Mathematical Modeling Biodynamic Response to Impact, pp. 31-44, 1976.

41. Ewing, C. L. and Thomas, D. J.: Human head and neck response to impact acceleration. Naval Aerospace Medical Laboratory, NAMRL Monograph 21, August, 1972.

SECURITY CLASSIFICATION OF THIS PAGE (When Data Entered)

REPORT DOCUMENTATION PAGE

READ INSTRUCTIONS BEFORE COMPLETING FORM

1. REPORT NUMBER: N00014-75-C-0372	2. GOVT ACCESSION NO.
3. RECIPIENT'S CATALOG NUMBER	
4. TITLE (and Subtitle): BIOENGINEERING MEASUREMENT	5. TYPE OF REPORT & PERIOD COVERED: Final Report
	6. PERFORMING ORG. REPORT NUMBER
7. AUTHOR(s): Albert I. King	8. CONTRACT OR GRANT NUMBER(s): N00014-75-C-0372
9. PERFORMING ORGANIZATION NAME AND ADDRESS: Wayne State University, Biomechanics Research Ctr. 418 Health Sciences Bldg., 1400 Chrysler Fwy. Detroit, Michigan 48202	10. PROGRAM ELEMENT, PROJECT, TASK AREA & WORK UNIT NUMBERS: NR105-540
11. CONTROLLING OFFICE NAME AND ADDRESS: Dept. of the Navy, Office of Naval Research Biophysics Program, Code 444	12. REPORT DATE: March 1, 1977
	13. NUMBER OF PAGES: 65
14. MONITORING AGENCY NAME & ADDRESS (if different from Controlling Office): same as above	15. SECURITY CLASS. (of this report): unclassified
	15a. DECLASSIFICATION/DOWNGRADING SCHEDULE

16. DISTRIBUTION STATEMENT (of this Report)

Approved for public release; distribution unlimited

17. DISTRIBUTION STATEMENT (of the abstract entered in Block 20, if different from Report)

same

18. SUPPLEMENTARY NOTES

19. KEY WORDS (Continue on reverse side if necessary and identify by block number)

$+G_z$ acceleration, pilot ejection, spinal hyperextension, spinal injury mechanism, articular facet load, intervertebral load, electromyography, neuromuscular delay, abdominal pressure, spinal mathematical models, vertebral fracture, cadaver experiments

20. ABSTRACT (Continue on reverse side if necessary and identify by block number)

This report discusses the mechanism and modelling of vertebral injuries resulting from emergency egress from disabled aircraft. The Ewing hypothesis states that posterior structures of the spine act as motion limiters which favor the occurrence of the commonly observed anterior wedge fractures. This hypothesis was verified in human cadavers and it was shown that the fracture g-level could be increased considerably by moderately hyperextending the spine with a 5 cm thick wooden block placed behind L1. The existence of a second

DD FORM 1 JAN 73 1473 EDITION OF 1 NOV 65 IS OBSOLETE S/N 0102-014-6601

L1.

SECURITY CLASSIFICATION OF THIS PAGE (When Data Entered)

load path via the articular facets was demonstrated quantitatively and the role of abdominal pressure as a third load path was found to be feasible but not effective at high g-levels encountered during ejection.

The effect of muscular response was studied using unanesthetized dogs which were subjected to low acceleration levels of 3 to 5g. Electromyography (EMG) was used to determine neuromuscular delay and the shape of the EMG derived muscle force-time curve.

A two-dimensional mathematical model of the spine was developed and validated against cadaveric data acquired under this study. The model was able to simulate spinal response reasonably well and predicted that the vertebral bodies in the lower thoracic region sustained the highest load during $+G_z$ acceleration.

There is now a better understanding of the mechanism of spinal injury which is not one of simple compressive failure. The ability of the facets to act as a load bearing structure of the spine has important implications in the mechanism of vertebral body fracture. The restraint system can be used to change the proportion of load carried by the vertebral bodies and thus increase the g-level for fracture.

+ G sub z